*Journal of Integrative Agriculture 2026, 25(3): 918–937*

KeAi
CHINESE ROOTS
GLOBAL IMPACT

**Available online at ScienceDirect**

**Journal of Integrative Agriculture**



RESEARCH ARTICLE

# Underlying mechanisms of high carbon budget surplus in low-stubble rice ratooning in Southeast China

**Qiaohong Fan[1], Jingnan Zou[1], Zhimin Lin[1], Gui Chen[1], Wu You[2], Kai Su[1#], Wenxiong Lin[1#]**

[1] *Institute of Agroecology, Fujian Agriculture and Forestry University, Fuzhou 350002, China*
[2] *Fujian Agricultural Ecological Environment and Energy Technology Extension Station, Fuzhou 350002, China*

## Highlights

- Ratoon rice maintains a higher carbon surplus compared to single- and double-cropping systems.
- This advantage arises from greater daily yields and lower greenhouse gas (GHG) emissions.
- A key mechanism involves preferential allocation of photosynthates to ratoon panicles rather than roots or soil.

## Abstract

The rice ratooning system has attracted increasing attention in southern China due to its low carbon emissions and high yield potential. However, the net carbon budget and underlying mechanisms remain unclear. Three rice cropping systems were established in this trial experiment conducted from 2021 to 2022 in Fuzhou (25°05′N, 119°13′E), Southeast China: ratooning rice (RR: MC+RSR) pattern for rice ratooning, single-cropping rice ($LR_1$), and double-cropping rice (DC: ER+$LR_2$). The closed static dark box gas collection, dry matter determination, life cycle assessment (LCA) etc. approaches were utilized to investigate the mechanism of "high carbon fixation–low emissions" mechanism in RR. A comprehensive assessment was conducted across multiple dimensions, including crop yield, greenhouse gas (GHG) emissions, carbon and nitrogen footprints, resource use efficiency, carbon sequestration capacity, and carbon budget balance. Results showed that the average daily yield of ratoon season rice (RSR) across RR treatments from 2021 to 2022 was 28.21–47.40% higher than that of the main crop (MC) and $LR_1$, and the average daily yield of RR was 13.50–27.76% higher than DC. This yield advantage was attributed to a 32.32–39.26% increase in the allocation of $^{13}C$-labeled photosynthetic products (including non-structural carbohydrates, NSCs) to panicle organs, and a 21.77–43.51% reduction in allocation to underground roots and soil. Furthermore, the average daily global warming potential (GWP) was 16.44 kg $CO_2$-eq $ha^{-1}$ for RR, 24.99 kg $CO_2$-eq $ha^{-1}$ for $LR_1$, and 21.32 kg $CO_2$-eq $ha^{-1}$ for DC. Specifically, the average daily GWP of ratoon rice was 34.21% lower than that of $LR_1$ and 22.90% lower than double-cropping rice. Similarly, the average daily greenhouse gas intensity (GHGI) of ratoon rice was 62.28% lower than $LR_1$ and 28.96% lower than double-cropping rice. In terms of carbon and nitrogen footprints, the ratoon rice system exhibited average daily values of 34.54 kg $CO_2$-eq $ha^{-1}$ and 0.47 kg N $ha^{-1}$, respectively. In comparison, $LR_1$ had values of 45.63 kg $CO_2$-eq $ha^{-1}$ and 0.49 kg N $ha^{-1}$, while double-cropping rice showed 43.38 kg $CO_2$-eq $ha^{-1}$ and 0.53 kg N $ha^{-1}$. These values represent reductions of 24.30% in carbon footprint and 4.28% in nitrogen footprint relative to $LR_1$, and 20.38 and 11.45% relative to double-cropping rice, respectively. Moreover, the average annual carbon budget surplus across systems was 22,380.01 kg $CO_2$-eq $ha^{-1}$ for ratoon rice (MC+RSR), 11,228.54 kg $CO_2$-eq $ha^{-1}$ for $LR_1$, and 23,772.15 kg $CO_2$-eq $ha^{-1}$ for DC. Consequently, the resource utilization efficiency of the RR was 24.42 and 47.50% higher than that of single-cropping and double-cropping systems, respectively. Average daily economic returns also increased by 32.71 and 80.75%, respectively. These findings provide a robust theoretical foundation and practical guidance for advancing agricultural carbon neutrality technologies and ensuring food security.

**Keywords:** carbon budget balance, carbon fixation and emission mitigation, carbon and nitrogen footprints, ratooning rice, single cropping rice, double cropping rice

Received 7 April 2025; Received in revised form 9 June 2025; Accepted 16 June 2025; Available online 7 July 2025
[#]Correspondence Kai Su, E-mail: fjsk1311@fafu.edu.cn; Wenxiong Lin, E-mail: wenxiong181@163.com

© 2026 CAAS. Publishing services by Elsevier B.V. on behalf of KeAi Communications Co. Ltd. This is an open access article under the CC BY-NC-ND license (http://creativecommons.org/licenses/by-nc-nd/4.0/). Peer review under responsibility of Editorial Board of *Journal of Integrative Agriculture*.
doi: 10.1016/j.jia.2025.07.012

## 1. Introduction

Rice is one of the world's most crucial food crops, sustaining more than half of the global population (Xu *et al.* 2018). Given continued population growth, the global population is projected to reach 9 billion by 2050, necessitating a greater than 50% increase in rice production to meet rising food demand (Yu *et al.* 2023). However, modern agricultural systems — particularly irrigated rice paddies — are major anthropogenic sources of methane emissions. This agriculture-climate feedback loop intensifies atmospheric warming and induces yield volatility, threatening global food security. Agricultural greenhouse gas emissions constitute a significant fraction of total anthropogenic emissions, with net $CH_4$ emissions from agriculture accounting for over 20% of global greenhouse gas totals. Of these, methane emissions from rice paddies represent 38% of anthropogenic $CH_4$ emissions (Yu *et al.* 2017; Cui *et al.* 2018; Qu *et al.* 2020; Chen *et al.* 2021). Therefore, reducing $CH_4$ emissions from rice paddies while maintaining stable yields is essential for achieving sustainable development that ensures both food security and environmental integrity. To this end, breeders and agronomists are actively developing and promoting high-yield, low-emission rice varieties aimed at simultaneously maximizing grain output and minimizing paddy-derived carbon emissions (Jiang *et al.* 2018, 2022; Zhang *et al.* 2021). Notably, rice production can function as either a "carbon source" or a "carbon sink". The carbon sink capacity of rice refers to its ability to fix $CO_2$ through photosynthesis and convert it into carbohydrates, thereby sequestering carbon in biomass and soil. This process comprises three components: plant carbon sequestration, root exudate carbon input, and soil organic carbon accumulation (Lin *et al.* 2015; Fang and Cheng 2018; Lin 2019; Chen *et al.* 2023; Yao *et al.* 2024). Conversely, the carbon source role encompasses all direct and indirect carbon emissions across the entire rice production lifecycle. Direct emissions include greenhouse gases — $CO_2$, $CH_4$, and $N_2O$ — released from the paddy ecosystem during crop growth, contributing approximately 60% of total emissions. Indirect emissions arise from supply chain inputs such as seeds, fertilizers, pesticides, plastic films, fuel, and electricity, quantified *via* life cycle assessment (LCA), and account for about 40% of total emissions. These indirect fluxes often co-occur with nitrogen footprints due to synthetic nitrogen applications. The balance between carbon sequestration and emissions in rice systems is evaluated using net ecosystem carbon budget (NECB) analysis. Positive NECB values indicate that carbon sequestration exceeds emissions, classifying the system as a carbon sink — primarily through accumulation of soil organic carbon (SOC) in paddy soils. Negative NECB values denote a net carbon source, predominantly driven by $CH_4$ emissions from anaerobic decomposition. These carbon flux regimes are governed by two key factors: (1) genotype-specific traits such as photosynthetic efficiency and root exudate composition, and (2) agroecosystem conditions influenced by management practices, particularly water regime and fertilizer application, which modulate soil redox potential and microbial metabolic pathways. Previous research has primarily focused on greenhouse gas emissions and cultivation strategies across different rice planting patterns — including double-cropping rice (DC), single-cropping rice ($LR_1$), and ratooning rice (RR) — and has established rice as a major contributor to agricultural carbon emissions, responsible for up to 55% of sector-wide totals (Stocker *et al.* 2013; Qian *et al.* 2023). Double-cropping and single-cropping systems are especially associated with high carbon emissions, particularly $CH_4$ (Qian *et al.* 2023; Li *et al.* 2024). In contrast, RR generally exhibits lower carbon emission intensity and reduced carbon and nitrogen footprints compared to other systems, positioning it as an environmentally favorable model (Lin *et al.* 2015; Ren *et al.* 2023). Nevertheless, some studies report elevated emissions in RR, particularly one month before and after main crop (MC) harvest, due to applications of bud-promoting and seedling-stimulating fertilizers that trigger $N_2O$ emissions — accounting for up to 70% of total emissions in some cases — and result in low nitrogen use efficiency. Thus, optimizing fertilization techniques is critical for achieving stable, high-yield, low-emission, and efficient RR production (Lin *et al.* 2024; Zou *et al.* 2024).

In recent years, advancements in RR varieties and improvements in supporting cultivation technologies — such as mechanical harvesting, low stubble retention, water-saving irrigation, minimized soil compaction, and loss reduction — have enabled the mechanized cultivation of RR to become the primary system promoted in southern China. This region possesses adequate temperature and light for one full growing season but insufficient conditions for reliable double cropping. As a result, RR has achieved consistently high grain yields per unit area (Chen *et al.* 2023). The estimated suitable area for RR cultivation in China is approximately $5.33\times10^6$ ha (Lin *et al.* 2015; Fang and Cheng 2018; Lin 2019; Chen *et al.* 2023; Yao *et al.* 2024), indicating substantial potential for enhancing national grain production. Further evidence indicates that, compared to DC, the RR system reduces overall carbon emissions by more than 40%. This reduction is largely attributable to the ratoon season rice (RSR) phase, which produces 90% less $CH_4$ than late-season rice in DC systems, while exhibiting daily productivity increases exceeding 30%. Consequently, RR demonstrates high daily productivity coupled with low carbon emissions. However, its net carbon budget — whether it functions as a net carbon source or sink — remains unclear (Lin Z *et al.* 2022), and comparative assessments with other rice cultivation systems are lacking. Initial findings suggest that Chinese rice paddies emit a net 195.49 Tg $CO_2$-eq annually (Tang *et al.* 2022). Existing studies show that the NECB of various rice systems ranges from 9,460 to 10,087 kg $CO_2$-eq $ha^{-1}$ (Ceschia *et al.* 2010; Wei *et al.* 2018), indicating variable roles as either carbon sources (negative values) or sinks (positive values). We hypothesize that these discrepancies may stem from differences in rice cultivars, cultivation environments, and methodological approaches (Mandal *et al.* 2021; Zhao *et al.* 2024). Prior studies have compared greenhouse gas emissions between RSR and its MC or $LR_1$, but comparison groups are limited. Moreover, comparisons between MC and RSR are confounded by differing growing seasons (early *vs.* late) and establishment

methods (transplanting *vs*. ratooning). Thus, distinguishing the underlying causes of observed differences remains challenging. Additionally, current research has overlooked comprehensive evaluations of the carbon budget balances and associated mechanisms across major rice cultivation systems — RR, $LR_1$, and DC — using locally adapted varieties selected under similar photothermal conditions (Huang *et al.* 2020; Wang *et al.* 2020; Lin F *et al.* 2022; Yuan *et al.* 2022; Chen *et al.* 2023; Yu *et al.* 2023; Deng 2024; Li *et al.* 2025). This gap risks systematic overestimation or underestimation of carbon sequestration and emission reduction potentials in RR and related systems (Qian *et al.* 2025), underscoring the need for rigorous, comparative research.

The "dual carbon" goals — peaking carbon dioxide emissions before 2030 and achieving carbon neutrality by 2060 — are central to China's pursuit of high-quality agricultural development. Agricultural carbon trading serves not only as a strategic instrument for meeting these targets (Wang and Peng 2018; Li *et al.* 2021; Lin *et al.* 2021; Wang 2021; Lin Q *et al.* 2022; Yang *et al.* 2023) but also as a pathway to enhance eco-economic benefits in farming systems. Pilot agricultural carbon trading programs in China have made notable progress, enabling farmers to realize economic returns through carbon sequestration projects in afforestation, tea plantations, wetlands, and bamboo forests. Reports from regions such as Sichuan, Zhejiang, and Fujian indicate carbon trading prices ranging from 20 to 60 CNY $t^{-1}$, effectively transforming ecological services into tangible income with considerable efficiency (Xu *et al.* 2015; Ling *et al.* 2019; Nakano *et al.* 2021; Zhang *et al.* 2023). To address declining grain self-sufficiency in southern China and strengthen regional food security, RR has emerged as a key strategy in implementing the new 50,000-t grain production plan in these areas. Accelerating research and thorough evaluation of greenhouse gas emission profiles and carbon budget balances across mechanical harvesting and low-stubble RR systems — and their comparative performance relative to DC and $LR_1$ — is therefore of significant theoretical and practical importance. Such work will support the implementation of the national grain production capacity enhancement initiative, ensuring food security while advancing reductions in agricultural carbon emissions toward the dual carbon goals. Accordingly, to enable a valid comparison of carbon budget characteristics among RR, $LR_1$, and DC rice systems, this study applied LCA methodology and selected two RR varieties with distinct genetic traits and growth durations. A two-year field experiment was conducted in southeastern China to assess carbon dynamics and agronomic performance across three contrasting systems: (i) RR (with early- and late-maturing varieties, including MC and RSR), (ii) $LR_1$ synchronized with RSR, particularly during the grain-filling stage, and (iii) DC systems. Through comparative analysis of yield components, $CH_4$/$N_2O$ fluxes, and NECB, this research elucidates the tradeoffs between carbon sequestration and emissions across different cultivation paradigms, providing a methodological framework for designing climate-smart rice production systems that optimize yield-carbon synergies.

## 2. Materials and methods

### 2.1. Research site and experimental design

The study was conducted at the experimental base of Fujian Agriculture and Forestry University in Fuzhou, Fujian Province, Southeast China (26°05′N, 119°13′E), with an average elevation of 12 m. The region has a subtropical monsoon climate. The rice varieties evaluated included the mid-maturing *indica* hybrid Taifengyou 3301 (TFY3301; total growth duration 120–130 d), the *indica–japonica* hybrid Yongyou 2640 (YY2640; 120–130 d), the mid-early maturing *indica* conventional Nanling 1 (NL1; 115–120 d), and the early-maturing Jiafuzhan (JFZ; 100–115 d). Three rice cropping systems were established: the RR system, the $LR_1$ system, and the DC system. In the RR system, two main crops were tested — mid-maturing RR (TFY3301-RR) and mid-early maturing RR (NL1-RR) — with subsequent RSR regrowth. The $LR_1$ system involved growing the same genotypes (TFY3301 and NL1) as single-crop mid-late rice harvested in the late season. Notably, in the RR system, the MC is classified as mid-late maturing early rice because it is harvested during the early season. To enable valid comparisons, the $LR_1$ treatment was managed so that its heading and grain-filling periods synchronized with those of the corresponding RSR.

The yield and greenhouse gas emission differences between RSR and $LR_1$ primarily arise from axillary bud activation mechanisms mediated by signaling pathways, particularly stubble cutting in ratooning cultivation. Comparative analyses between the MC (early season) and RSR (late season) reflect how the same genotype responds physiologically to differing temperature and light environments across seasons. Furthermore, integrated comparisons among RR, $LR_1$, and DC rice systems were conducted to assess their carbon and nitrogen footprints and associated eco-economic benefits under regional light-temperature constraints. This experiment aims to elucidate the carbon sequestration and emission reduction characteristics of RR and their underlying formation mechanisms through targeted field designs and comparative assessments (Appendices A and B). The field experiment followed a randomized block design with three replicates. Each plot measured 100 $m^2$, subdivided into randomized 20 $m^2$ experimental units. The soil type was clay loam paddy soil. Initial soil properties in 2021 were as follows: pH 5.3, total nitrogen 1.42 g $kg^{-1}$, available phosphorus 22.83 mg $kg^{-1}$, available potassium 150.00 mg $kg^{-1}$, and organic matter content 2.10%. In 2022, values were pH 5.1, total nitrogen 2.16 g $kg^{-1}$, available phosphorus 25.47 mg $kg^{-1}$, available potassium 143.24 mg $kg^{-1}$, and organic matter 2.27%. All varieties were sown on March 25 and transplanted on April 25 in both years, with uniform spacing of 30 cm×15 cm and three seedlings per hill (three grains/hill). Plots were separated by small dikes and equipped with independent irrigation and drainage systems. Nitrogen fertilizer for the MC was applied in the ratio basal:tillering:panicle:grain=3:2:3:2. Total nitrogen (as urea, converted to pure N) was 225 kg N $ha^{-1}$, except for the shorter-duration NL1-MC, which received 200 kg N $ha^{-1}$. Phosphorus fertilizer (12.0% $P_2O_5$) was applied

solely as basal dressing at 562.5 kg ha$^{-1}$, while potassium fertilizer (60.0% $K_2O$) was split equally between basal and grain fertilizer, totaling 300 kg ha$^{-1}$. Fertilization for $LR_1$ mirrored that of the respective MC treatments (NL1-$LR_1$ and Taifengyou 3301 mid-maturing *indica* hybrid rice (TFY3301-$LR_1$ were sown on June 5). For RSR, nitrogen was applied in two splits — 3 days after MC harvest and at heading — in a 3:1 ratio, totaling 120 kg N ha$^{-1}$. In the DC system, early rice (ER; JFZ) received 180 kg N ha$^{-1}$, and late rice ($LR_2$; YY2640) received 200 kg N ha$^{-1}$. Other field management practices followed conventional recommendations. Pest and disease control was maintained throughout the growing period. To minimize herbicide impacts on soil microorganisms, manual weeding was implemented to prevent weed competition and potential yield loss. In both 2021 and 2022, NL1-MC was manually harvested on July 25 and that of TFY3301 main crop (TFY3301-MC) on August 5, leaving a 15 cm stubble height. When grown as $LR_1$, NL1 and TFY3301 were sown on June 5 to ensure heading synchronization with their corresponding RSR counterparts. Two additional comparator sets with distinct growth durations were synchronized to head on September 5 and September 15, respectively. Double-cropping early rice (DC-JFZ early maturing rice (JFZ-ER) was harvested on July 5, and double-cropping late rice (YY2640-$LR_2$) on October 5.

### 2.2. Determination of yield and its components

At maturity, 20 rice plants per treatment were randomly selected to evaluate grain yield and its components, including number of effective panicles, grains per panicle, seed setting percentage, and 1,000-grain weight.

### 2.3. Determination of non-structural carbohydrates (NSCs) content

Three representative plants at the heading and maturity stages were selected and sampled from different rice varieties and cropping patterns. The plants were surface-rinsed with water and separated into roots, stem sheaths, stubble, leaves, and panicles. Each organ sample was transferred to a paper bag, oven-dried and deactivated at 105°C for 30 min, then dried at 70°C to constant weight. The dried samples were ground and sieved. Soluble sugar and starch contents in stem sheaths at the heading and maturity stages were determined following the protocol of Yoshida *et al.* (1971).

The NSC content (comprising soluble sugars and starch) in different plant parts was quantified using the method described by Zou *et al.* (2024). NSC accumulation per plant part was calculated as the product of NSC concentration and corresponding dry weight.

The NSC translocation amount (mg/plant by organ) was estimated as the difference between NSC content at the heading stage and NSC content at the maturity stage (eq. (1)): NSC translocation amount (mg/plant by organ)=NSC content at heading stage–NSC content at maturity stage (1)

The NSC translocation rate (%) was calculated according to eq. (2): NSC translocation rate (%)=(1–NSC content at maturity stage/NSC content at heading stage)×100 (2)

The contribution of translocated NSC to grain yield (%) was determined using eq. (3): NSC contribution rate to grain (%)=(NSC content at heading stage–NSC content at maturity stage)/Grain weight at maturity stage×100 (3)

### 2.4. $^{13}C$ pulse labeling

To further confirm the $^{13}C$ photoassimilate partitioning properties of RR, pot experiments were conducted using plastic pots (33 cm height×20 cm diameter) filled with field soil collected in 2022. Plants were grown in a controlled-environment chamber maintained at 22°C with a 16-h light/8-h dark cycle. Three seedlings were transplanted per pot following standard agronomic practices. $^{13}CO_2$ labeling was performed in transparent cylindrical acrylic chambers, each consisting of a cylindrical body with a detachable lid. The chambers were equipped with internal circulation fans and external gas sampling ports. Pulse labeling was conducted at the synchronizing heading stage for MC, RSR, and $LR_1$ of TFY3301 and NL1. Prior to labeling, plants were placed in the chambers and allowed to photosynthesize under ambient light to deplete endogenous $^{12}CO_2$ and enhance subsequent $^{13}CO_2$ assimilation. Labeling commenced by injecting $^{13}CO_2$ (>99 atom%, Shanghai Institute of Chemical Industry) while operating the circulation fans. Following the 8-h labeling period, ambient $CO_2$ was introduced to promote $^{13}C$ fixation and minimize $^{13}CO_2$ loss. Control plants were maintained 10 m away from the labeling area under identical environmental conditions to determine background natural $^{13}C$ abundance. The $^{13}CO_2$ pulse labeling protocol followed that described by Li *et al*. (2022). Soil, different plant parts, and weekly gas samples were analyzed using an elemental analyzer, high-temperature conversion system, and isotope ratio mass spectrometer (EA/HT-IRMS, Thermo Fisher Scientific, Bremen, Germany). The $^{13}C/^{12}C$ ratios were measured, and $\delta^{13}C$ values were calculated relative to the international Pee Dee Belemnite (PDB) standard. Total carbon content (C%) was determined by comparing sample peak areas with those of working standard samples (Zou *et al*. 2024).

### 2.5. Determination of greenhouse gas emissions

In the two-year field experiment conducted from April 2021 to November 2022, greenhouse gas samples were collected every 7–10 days between 9 a.m. and 12 p.m. following transplanting in the RR (MC+RSR), DC (ER+$LR_2$), and $LR_1$ (synchronous heading with RSR). Each gas sampling chamber was secured using a stainless steel base measuring 40 cm×22 cm×12 cm, inserted into the soil to a depth of approximately 10 cm. The chamber, constructed from transparent acrylic plates (40 cm long×22 cm wide×100 cm high), included a thermometer and a 12 V battery-powered fan connected to a power bank to ensure uniform air mixing during sampling. A sealed gas sampling port was installed and opened only during sample collection. Gas samples were collected at 0, 10, 20, and 30 min after chamber closure using a 50 mL syringe attached to a stopcock and immediately transported to the laboratory. The samples were injected into 30 mL pre-evacuated vials and analyzed *via* gas chromatography (Agilent 7890B, USA) to determine

concentrations of $CO_2$, $CH_4$, and $N_2O$. $CH_4$ and $CO_2$ were quantified using a flame ionization detector (FID), while $N_2O$ was measured using a micro electron capture detector (ECD) operated at 200°C. The column temperature was maintained at 55°C, and calibration was performed using standard gases from laboratory-stored cylinders. Greenhouse gas fluxes were then calculated for each sampling event to enable comparative analysis across cropping systems (Appendix B) (Yu *et al.* 2023).

The greenhouse gas emission flux is calculated using the following formula:

$$F=60\times h\times \frac{Mw\times 273.15}{22.41\times(273.15+T)}\times\frac{dC}{dT} \quad (4)$$

where F represents the greenhouse gas emission flux (mg $m^{-2}$ $h^{-1}$); 60 is the conversion factor to express the time unit in hours; h denotes the height of the gas sampling chamber (m); T is the average chamber temperature during sampling (°C); Mw is the molar mass of the target gas (g $mol^{-1}$); and dC/dT is the rate of gas concentration change over time ($1\times10^{-6}$ L $L^{-1}$, equivalent to ppmv $min^{-1}$).

Total cumulative greenhouse gas emissions are computed using the formula:

$$f=\sum_{i=1}^{n}\left(\frac{F_i+F_{i-1}}{2}\times D\times 24\times 0.01\right) \quad (5)$$

where $f$ denotes the total greenhouse gas emission (kg $ha^{-1}$), $n$ is the total number of gas sampling events, $F_i$ and $F_{i-1}$ represent the flux values of the measured greenhouse gas during the $i$th and ($i$–1)th sampling events, respectively (mg $m^{-2}$ $h^{-1}$), and D is the time interval in days between consecutive sampling events (d).

## 2.6. Measurement of global warming potential and greenhouse gas intensity

The global warming potential (GWP) quantifies the radiative impact of greenhouse gases relative to $CO_2$. Over a 100-year time horizon, the GWPs for $CH_4$ and $N_2O$ are 25 and 298, respectively. To calculate total $CO_2$ equivalent emissions, the following formula is used to determine the GWP of greenhouse gas (GHG) emissions from rice fields (Li *et al.* 2025):

$$GWP=25\times f(CH_4)+298\times f(N_2O) \quad (6)$$

where GWP denotes the global warming potential value (kg $CO_2$-eq $ha^{-1}$), and $f(CH_4)$ and $f(N_2O)$ represent the total emissions of $CH_4$ and $N_2O$, respectively.

The greenhouse gas intensity (GHGI) is calculated using the equation below (Li *et al.* 2025):

$$GHGI=GWP/Y \quad (7)$$

where GHGI represents carbon emission intensity (kg $CO_2$-eq $t^{-1}$); GWP denotes total greenhouse gas emissions during the growing season in $CO_2$ equivalent (kg $CO_2$-eq $ha^{-1}$), and Y denotes rice yield (t $ha^{-1}$).

To enable a more transparent comparison of GHG emission intensities among RR, $LR_1$, and DC systems, the study applied the aforementioned equations to quantify individual GHG emission intensities, defined as the total amount of $CO_2$, $CH_4$, and $N_2O$ emitted per ton of rice produced per hectare (kg $t^{-1}$).

$$GHGI(CO_2)=f(CO_2)/Y \quad (8)$$

$$GHGI(CH_4)=f(CH_4)/Y \quad (9)$$

$$GHGI(N_2O)=f(N_2O)/Y \quad (10)$$

In these equations, $GHGI(CO_2)$, $GHGI(CH_4)$, and $GHGI(N_2O)$ denote the emission intensities of $CO_2$ (kg $CO_2$ $t^{-1}$), $CH_4$ (kg $CH_4$ $t^{-1}$), and $N_2O$ (kg $N_2O$ $t^{-1}$), respectively; $f(CO_2)$ ($f(CH_4)$, and $f(N_2O)$ denote the total emissions of $CO_2$ (kg $CO_2$ $ha^{-1}$), $CH_4$ (kg $CH_4$ $ha^{-1}$), and $N_2O$ (kg $N_2O$ $ha^{-1}$), respectively.

## 2.7. Measurement of resource use efficiency and carbon-nitrogen footprints

To evaluate the resource use efficiency of three rice cultivation patterns adapted to different climate zones — mid-early and mid-late RR, $LR_1$ under RSR-synchronous heading control, and DC — this study conducted resource use accounting based on measured agronomic inputs and grain yield, calculating net energy and resource use efficiency (Yu *et al.* 2023).

$$\text{Net energy=Energy output (GJ } ha^{-1}\text{)–Energy input (GJ } ha^{-1}\text{)} \quad (11)$$

$$\text{Resource use efficiency=Energy output (GJ } ha^{-1}\text{)/Energy input (GJ } ha^{-1}\text{)} \quad (12)$$

The environmental footprint was assessed by quantifying both indirect carbon emissions and reactive nitrogen losses, along with direct field-level emissions associated with agricultural inputs across production, processing, and transportation stages. Carbon footprint (CF), nitrogen footprint (NF), and nitrogen content were calculated using established methodologies (Yu *et al.* 2023). The formulas are as follows:

$$CF=CF_{indirect}+25\times CH_4+298\times N_2O \quad (13)$$

where CF denotes the carbon footprint per unit area (kg $CO_2$-eq $ha^{-1}$); $CF_{Indirect}$ is derived by multiplying each agricultural input — including machinery operation, labor, diesel, seeds, nitrogen fertilizer, phosphorus fertilizer ($P_2O_5$), potassium fertilizer ($K_2O$), pesticides, and electricity — by its corresponding $CO_2$ emission coefficient, with values sourced from Yu *et al.* (2023). The factors 25 and 298 represent the GWP of $CH_4$ and $N_2O$, respectively, over a 100-year time horizon.

$$NF=NF_{indirect}+NE_{N_2O}+NV_{NH_3}+NL_{NO_3^-}+NR_{NH_4^+} \quad (14)$$

$$NV_{NH_3}=2.97+0.16\times N\ rate \quad (15)$$

$$NL_{NO_3^-}=6.03e^{0.0048\times N\ surplus} \quad (16)$$

$$NR_{NH_4^+}=8.69e^{0.0077\times N\ surplus} \quad (17)$$

where NF represents the nitrogen footprint (kg N $ha^{-1}$), and $NF_{indirect}$ indicates indirect nitrogen loss, computed from agricultural inputs and their respective reactive nitrogen loss coefficients, as reported by Yu *et al.* (2023). $NE_{N_2O}$ ($N_2O$ emissions) encompasses both direct and indirect emissions: direct emissions were measured in field experiments, while indirect emissions were estimated as 20% of direct emissions. Reactive nitrogen losses — including ammonia volatilization ($NV_{NH_3}$), nitrogen leaching ($NL_{NO_3^-}$), and nitrogen runoff ($NR_{NH_4^+}$) — were quantified using nitrogen application rates or nitrogen surplus.

## 2.8. Measurement of net ecosystem economic benefit

The net ecosystem economic benefit (NEEB) is an integrative metric used to evaluate the economic efficiency of cropping

systems, as established in prior research (Yu *et al.* 2023). It accounts for both financial returns and environmental externalities through a comprehensive cost–benefit framework.

NEEB=Economic output–Agricultural input costs–Carbon footprint cost ($Cf_{cost}$)–Nitrogen footprint cost ($Nf_{cost}$) (18)

### 2.9. Measurement of carbon content and carbon budget balance

In the rice ecosystem, carbon sink, carbon source, carbon sequestration, and carbon consumption coexist. Rice production functions as both a carbon sink and a carbon source. In this study, the net ecosystem carbon balance (NECB, defined as the carbon budget surplus) was calculated by determining the difference between total carbon input and total carbon output within the farmland ecosystem:

$$NECB=C_{input}–C_{output} \quad (19)$$

Previous studies indicate that in paddy field ecosystems, long-term management practices such as straw incorporation and no-tillage enhance SOC storage (Lal 2004; Huang *et al.* 2021). However, because the duration of this study spanned only two growing seasons, changes in SOC stocks were not considered. Instead, the net primary productivity (NPP) of paddy fields was used as the primary carbon input to the ecosystem, calculated according to the following formula (Smith *et al.* 2010; Xu *et al.* 2022):

$$C_{NPP}=(C_S+C_L+C_G+C_R+C_r+C_E)\times\frac{44}{12} \quad (20)$$

where $C_{NPP}$ represents the $CO_2$ fixation associated with NPP, including contributions from stem biomass ($C_S$), leaf biomass ($C_L$), grain ($C_G$), root biomass ($C_R$), aboveground crop residue ($C_r$), and root exudates ($C_E$). The ratio 44/12 reflects the molar mass ratio of $CO_2$ to elemental carbon. Carbon output was quantified as the $CO_2$ equivalent of aboveground biomass removed from the system, encompassing grain carbon harvested, carbon losses due to heterotrophic respiration, and emissions of $CO_2$, $CH_4$, and $N_2O$. Thus, carbon output in this study was determined using the following eqs.:

$$C_{output}=C_{export}+GHG_{direct}+GHG_{indirect} \quad (21)$$

$$GHG_{direct}=CE_{CO_2}+25\times CE_{CH_4}+298\times CE_{N_2O} \quad (22)$$

$$GHG_{indirect}=\sum_{i=1}^{n} AI_i\times EF_i \quad (23)$$

where $GHG_{direct}$ denotes the carbon dioxide equivalent of direct GHG emissions, where 25 and 298 represent the GWP values of $CH_4$ and $N_2O$ over a 100-year time horizon, respectively (IPCC 2013). $GHG_{indirect}$ refers to the carbon dioxide equivalent of indirect greenhouse gas emissions arising from the use of agricultural inputs such as fertilizers, herbicides, pesticides, fungicides, seeds, diesel fuel, and electricity consumed during groundwater irrigation. $AI_i$ indicates the quantity of each agricultural input utilized in the cropping system; $EF_i$ is the corresponding emission factor, representing the rate of greenhouse gas emission per unit of input (Yao *et al.* 2024).

### 2.10. Statistical analysis

All measurement data were derived from at least three biologically independent replicates. Data were analyzed and visualized using Origin2024 software. One-way ANOVA was used with SPSS20.0, and post hoc mean comparisons were performed using Duncan's multiple range test at a significance level of $P<0.05$.

## 3. Results

### 3.1. Analysis of yield and its components

The findings indicate that RSR exhibited significant improvements in panicle number, seed setting percentage, 1,000-grain weight, and daily yield compared to both the MC in RR systems and the corresponding $LR_1$, across cultivars with varying maturity periods. As shown in Table 1, in 2021, the panicle counts in RSR derived from TFY3301 and NL1 (TFY3301-RSR and NL1-RSR) increased by 46.36 and 50.38%, respectively, relative to their respective MC (TFY3301-MC and NL1-MC). This enhancement represented increases of 42.75 and 32.41%, respectively, over those of single-cropped medium-late rice (TFY3301-$LR_1$ and NL1-$LR_1$). The seed-setting percentage of the panicles in TFY3301-RSR and NL1-RSR improved by 6.90 and 8.87 percentage points, respectively, compared to their MC counterparts; TFY3301-RSR showed a 12.75% higher seed-setting percentage than TFY3301-$LR_1$, while NL1-RSR exhibited a 5.35% lower value than NL1-$LR_1$. Similarly, the 1,000-grain weight increased by 3.41, 2.15, 3.41, and 2.29% across the comparisons. Furthermore, grain yield was reduced by 25.54, 6.85, 25.69, and 16.39%, respectively, relative to the MC and $LR_1$ controls. In contrast, daily yield — reflecting yield efficiency per growing day — increased by 29.08, 42.84, 28.81, and 28.21%, respectively, as detailed in Table 1.

The experimental results obtained in 2022 were consistent with those from the previous year. Specifically, the number of productive panicles in TFY3301-RSR and NL1-RSR increased by 39.40, 31.71, 46.20, and 41.66% compared to their MC (TFY3301-MC and NL1-MC) and $LR_1$ (TFY3301-$LR_1$ and NL1-$LR_1$) counterparts, respectively. The seed-setting percentage of TFY3301-RSR was 6.76% lower than that of its MC, whereas NL1-RSR showed an 11.43% increase relative to its MC. Compared with $LR_1$ controls, TFY3301-RSR and NL1-RSR exhibited improvements of 6.42 and 7.51%, respectively. Similarly, the 1,000-grain weight of TFY3301-RSR and NL1-RSR increased by 3.75, 3.57, 2.81, and 3.16% relative to their MC and $LR_1$ counterparts, respectively. Moreover, although grain yield was reduced by 22.10, 3.87, 24.43, and 13.24% compared to the MC and $LR_1$ controls, the daily yield of TFY3301-RSR and NL1-RSR increased by 35.03 and 47.42%, respectively, relative to their MC counterparts, and by 30.99 and 33.03% compared to the $LR_1$ (i.e., RSR synchronous heading) controls. Additionally, the RR system, particularly the mid-late maturity RR pattern, demonstrated superior total yield compared to the DC system. Specifically, the total yield from the TFY3301-RR was 17.08 and 17.31 t $ha^{-1}$ in 2021 and 2022, respectively, while the total yield of the NL1-RR was 14.39 and 14.71 t $ha^{-1}$ in the same years. In contrast, the total yield of the DC pattern was 14.68 and

**Table 1 Comparison of grain yield and its components among different varieties under MC, RSR, and $LR_1$ with RSR-synchronous heading conditions in 2021 and 2022**

| Year (Y) | Variety (V)[1)] | Cultivation pattern (C)[2)] | Panicles $m^{-2}$ | Spikelet number per panicle | Seed-setting percentage (%) | 1,000-grain weight (g) | Grain yield (t $ha^{-1}$) | Daily average grain yield (kg $ha^{-1}$ $d^{-1}$) |
|---|---|---|---|---|---|---|---|---|
| 2021 | TFY3301 | MC | 252.97 c | 207.33 a | 82.63 c | 22.61 a | 9.79 a | 75.30 b |
| | | RSR | 370.24 a | 95.46 d | 88.33 b | 23.38 a | 7.29 c | 97.20 a |
| | | $LR_1$ | 259.37 c | 213.72 a | 78.34 d | 22.61 a | 9.81 a | 75.46 b |
| | NL1 | MC | 190.33 e | 213.86 a | 80.48 cd | 22.75 a | 7.45 c | 64.78 c |
| | | RSR | 286.21 b | 102.53 d | 87.62 b | 23.24 a | 6.94 c | 92.53 a |
| | | $LR_1$ | 216.16 d | 182.78 b | 92.57 a | 22.72 a | 8.30 b | 72.17 b |
| | JFZ | ER | 208.30 de | 148.40 c | 82.41 cd | 22.26 a | 6.03 d | 60.03 c |
| | YY2640 | $LR_2$ | 197.89 de | 216.74 a | 79.34 cd | 22.44 a | 8.65 b | 72.08 b |
| 2022 | TFY3301 | MC | 282.38 bc | 187.63 b | 90.14 a | 22.93 a | 9.73 a | 74.84 b |
| | | RSR | 393.64 a | 96.37 d | 84.05 b | 23.79 a | 7.58 c | 101.06 a |
| | | $LR_1$ | 269.25 c | 203.87 a | 78.98 c | 23.14 a | 10.03 a | 77.15 b |
| | NL1 | MC | 226.38 de | 183.64 b | 80.65 bc | 22.38 a | 7.50 c | 65.21 cd |
| | | RSR | 298.16 b | 95.03 d | 89.87 a | 23.18 a | 7.21 c | 96.13 a |
| | | $LR_1$ | 210.47 ef | 189.36 b | 83.59 bc | 22.47 a | 8.31 b | 72.26 bc |
| | JFZ | ER | 231.25 d | 131.42 c | 83.62 bc | 22.53 a | 5.91 d | 59.10 d |
| | YY2640 | $LR_2$ | 207.82 f | 186.52 b | 79.45 cc | 23.46 a | 8.63 b | 71.91 bc |
| *F*-value | Y | | 27.999*** | 57.828*** | NS | NS | NS | NS | 27.999*** |
| | V | | 358.732*** | 7.847** | 6.836* | NS | 119.944*** | 24.781*** | 358.732*** |
| | C | | 348.875*** | 915.985*** | 11.816*** | NS | 73.387*** | 170.252*** | 348.875*** |
| | Y×V | | NS | NS | 4.907* | NS | NS | NS | NS |
| | Y×C | | 6.309** | 11.536*** | 8.813** | NS | NS | NS | 6.309** |
| | V×C | | 11.193*** | 13.999*** | 31.535*** | NS | 18.934*** | NS | 11.193*** |
| | Y×V C | | NS | 3.825* | 10.339*** | NS | NS | NS | NS |

[1)] TFY3301, YY2640, JFZ, and NL1 refer to the hybrid rice varieties Taifengyou 3301 and Yongyou 2640, and the conventional varieties Jiafuzhan and Nanling 1, respectively.
[2)] MC, main crop rice; RSR, ratoon season rice; ER, double-cropping early rice; $LR_1$, single-cropping mid-late rice with synchronous heading relative to RSR; $LR_2$, double-cropping late rice.
Different lowercase letters within the same column and year indicate significant differences determined by ANOVA ($P$<0.05). NS indicates no significant difference at the 0.05 probability level; ***, **, and * denote significances at the 0.001, 0.01, and 0.05 levels, respectively.

14.54 t $ha^{-1}$ in 2021 and 2022, respectively (Table 1). These yield differences are primarily attributable to variations in total growth duration among cropping systems and the inherent yield potential of the selected cultivar combinations.

### 3.2. Analysis of NSC and $^{13}C$ pulse labeling

The accumulation and distribution patterns of NSC under different cropping systems are presented in Table 2. In 2021, the NSC translocation rates in various tissues of RSR were significantly higher than those in MC and $LR_1$ with synchronous heading ($LR_1$). Specifically, root NSC translocation rates in TFY3301-RSR and NL1-RSR increased by 57.74 and 66.24%, respectively, compared to MC, and by 56.15 and 46.98% relative to $LR_1$. Similarly, stem NSC translocation rates rose by 101.88 and 94.27% over MC, and by 83.60 and 113.29% compared to $LR_1$. Leaf NSC translocation rates were also significantly elevated — by 75.15 and 65.93% relative to MC, and by 65.86 and 87.56% compared to $LR_1$. Furthermore, RSR exhibited a significantly greater yield contribution rate than both MC and $LR_1$.

In 2022, RSR continued to show significantly higher NSC translocation and yield contribution rates than MC and $LR_1$. Root NSC translocation rates in TFY3301-RSR and NL1-RSR were elevated by 93.24 and 80.07% relative to MC, and by 77.28 and 119.97% compared to $LR_1$, respectively. Stem NSC translocation rates increased by 89.41 and 97.11% over MC, and by 97.29 and 86.29% relative to $LR_1$. Additionally, RSR demonstrated a substantially higher yield contribution than either MC or $LR_1$.

$^{13}CO_2$ isotope labeling analysis further elucidated the allocation characteristics of photosynthetic assimilates across different rice cropping systems. As shown in Table 3, under TFY3301-RSR and NL1-RSR systems, the $^{13}C$ content in soil decreased by 78.26 and 39.89%, 77.69 and 45.54% compared to MC and $LR_1$ counterparts, respectively. The $^{13}C$ content in roots, stems-sheaths, and leaves declined by 16.44–28.08%, 14.28–30.72%, 52.64–62.00% and 45.71–63.35%, 20.09–24.15%, 14.88–21.43% relative to MC and $LR_1$. In contrast, the $^{13}C$ content in grains increased by 35.59–39.26% and 32.32–33.58% compared to MC and $LR_1$, respectively. These results indicate that, relative to MC and $LR_1$, $^{13}C$-labeled photosynthates in RSR were preferentially allocated to grains, with the highest partitioning observed in panicles and the lowest in soil. This pattern corroborates that dry matter allocation to panicle organs during critical growth stages is markedly enhanced in RR, resulting in a higher economic coefficient and increased daily yield. This physiological mechanism underpins the RR system's ability

**Table 2 Non-structural carbohydrates (NSC) translocation in MC, RSR, and $LR_1$ with RSR synchronous heading from 2021 to 2022**

| Year (Y) | Variety (V)[1] | Cultivation pattern (C)[2] | NSC translocation amount (mg/plant) | | | | NSC translocation rate (%) | | | | NSC contribution rate to grain (%) | | | |
|---|---|---|---|---|---|---|---|---|---|---|---|---|---|---|
| | | | Root | Stem | Leaf | Stubble | Root | Stem | Leaf | Stubble | Root | Stem | Leaf | Stubble |
| 2021 | TFY3301 | MC | 988.41 a | 2,463.19 c | 1,462.22 c | 98.13 b | 35.26 b | 32.43 b | 36.78 b | 65.47 b | 3.15 b | 7.85 b | 4.66 d | 0.42 b |
| | | RSR | 986.02 a | 3,380.97 a | 1,803.81 a | | 55.62 a | 65.47 a | 64.42 a | | 4.22 a | 14.47 a | 7.72 a | |
| | | $LR_1$ | 716.88 b | 2,270.13 cd | 1,880.25 a | | 35.62 b | 35.66 b | 38.84 b | | 2.28 c | 7.22 b | 5.98 c | |
| | NL1 | MC | 635.16 c | 2,058.30 d | 1,055.42 d | 122.34 a | 33.35 b | 35.44 b | 41.45 b | 69.25 a | 2.66 bc | 8.62 b | 4.42 d | 0.55 a |
| | | RSR | 1,034.33 a | 2,953.95 b | 1,552.60 bc | | 55.44 a | 68.85 a | 68.78 a | | 4.65 a | 13.28 a | 6.98 ab | |
| | | $LR_1$ | 707.63 b | 2,093.62 d | 1,713.21 ab | | 37.72 b | 32.28 b | 36.67 b | | 2.66 bc | 7.87 b | 6.44 bc | |
| 2022 | TFY3301 | MC | 785.88 c | 2,229.79 d | 1,662.21 b | 126.33 b | 32.54 bc | 33.82 b | 35.53 b | 65.77 a | 2.52 c | 7.15 b | 5.33 b | 0.52 b |
| | | RSR | 1,054.40 b | 3,544.62 a | 1,756.52 ab | | 62.88 a | 64.06 a | 67.52 a | | 4.34 b | 14.59 a | 7.23 a | |
| | | $LR_1$ | 729.75 d | 2,533.22 c | 1,761.68 ab | | 35.47 bc | 32.47 b | 30.76 b | | 2.27 c | 7.88 b | 5.48 b | |
| | NL1 | MC | 514.42 e | 1,663.46 f | 1,403.85 c | 140.96 a | 36.33 b | 34.27 b | 35.43 b | 62.68 a | 2.14 c | 6.92 b | 5.84 b | 0.61 a |
| | | RSR | 1,203.98 a | 3,195.97 b | 1,814.05 a | | 65.42 a | 67.55 a | 62.67 a | | 5.21 a | 13.83 a | 7.85 a | |
| | | $LR_1$ | 593.95 f | 1,896.38 e | 1,400.98 c | | 29.74 c | 36.26 b | 35.84 b | | 2.23 c | 7.12 b | 5.26 b | |
| *F*-value | | Y | 9.183** | NS | NS | 37.144*** | NS | NS | 8.871** | 4.317* | NS | NS | NS | 13.265** |
| | | V | 86.766*** | 98.316*** | 68.106*** | 25.553*** | NS | NS | NS | NS | NS | NS | NS | 24.801*** |
| | | C | 558.319*** | 301.503*** | 56.823*** | 4,030.832*** | 193.078*** | 296.296*** | 334.850*** | 7,614.210*** | 151.887*** | 148.830*** | 100.857*** | 2,185.862*** |
| | | Y×V | NS | 4.429* | NS | NS | NS | NS | NS | 5.194* | NS | NS | NS | NS |
| | | Y×C | 63.587*** | 12.496*** | 26.329*** | 37.144*** | 7.897** | NS | NS | 4.317* | 5.401* | NS | 15.046*** | 13.265*** |
| | | V×C | 135.883*** | NS | 6.249** | 25.553*** | NS | NS | NS | NS | 7.352** | NS | NS | 24.801*** |
| | | Y×V×C | 12.692*** | NS | 6.998** | NS | 3.888* | NS | 5.240* | 5.194* | NS | NS | 4.661* | NS |

[1] TFY3301 and NL1 refer to the hybrid rice variety Taifengyou 3301 and the conventional variety Nanling 1, respectively.
[2] MC, main crop rice; RSR, ratoon season rice; $LR_1$, single-season mid-late rice with synchronized heading relative to RSR.
Different lowercase letters within the same column and year indicate significant differences (ANOVA, $P<0.05$). NS indicates no significant difference at the 0.05 probability level; ***, **, and * denote significant differences at the 0.001, 0.01, and 0.05 probability levels, respectively.

to achieve two harvests from a single planting, particularly its superior daily productivity compared to $LR_1$ and DC systems (Tables 1–3; Appendix C).

### 3.3. Analysis of GHG emission fluxes

In the period from 2021 to 2022, GHG emission fluxes under different rice cropping patterns were closely associated with rice plant growth and development, exhibiting an initial increase followed by a decrease, accompanied by fluctuations (Fig. 1). Specifically, the $CO_2$ and $CH_4$ emission peaks for MC and $LR_1$ occurred around the booting and grain filling stages, whereas the primary emission peaks for RSR were observed within 10 to 15 days after harvest. Compared to MC and $LR_1$, RSR exhibited significantly lower cumulative $CO_2$, $CH_4$, and $N_2O$ emission fluxes. Relative to DC systems, RR showed significantly lower cumulative $CO_2$ and $CH_4$ emissions. However, cumulative $N_2O$ emissions depended on the growth duration of RR cultivars: TFY3301-RR exhibited a marked increase in $N_2O$ emission fluxes, whereas the NL1-RR experienced a significant decrease. Notably, cumulative $CH_4$ emissions from RR were consistently lower than those from $LR_1$.

In 2021, the annual cumulative $CO_2$ emission fluxes from TFY3301-RSR were 49.19 and 42.70% lower than those of its MC and $LR_1$ counterparts, respectively. In contrast, the TFY3301-RR system emitted 70.07% more $CO_2$ than $LR_1$ and 8.38% more than DC. For NL1-RSR, $CO_2$ emissions decreased by 58.61 and 55.92% relative to MC and $LR_1$, respectively. The corresponding NL1-RR system emitted 50.56% more $CO_2$ than $LR_1$ but 19.77% less than DC. In 2022, cumulative $CO_2$ emissions from TFY3301-RSR were reduced by 36.05 and 49.51% compared to MC and $LR_1$, respectively. The TFY3301-RR system emitted 29.45% more $CO_2$ than $LR_1$ but 19.78% less than DC. Similarly, NL1-RSR recorded reductions of 52.27 and 51.81% relative to MC and $LR_1$. The NL1-RR system showed a 49.15% increase compared to $LR_1$, yet a 7.95% reduction relative to DC.

In 2021, annual cumulative $CH_4$ emission fluxes from TFY3301-RSR were reduced by 95.25 and 94.58% compared to MC and $LR_1$, respectively. The TFY3301-RR system emitted 19.75% more $CH_4$ than $LR_1$ but 15.81% less than DC. For NL1-RSR, emissions declined by 88.10 and 49.48% relative to MC and $LR_1$, respectively. The corresponding NL1-RR system showed reductions of 1.07 and 33.96% compared to $LR_1$ and DC. In 2022, $CH_4$ emissions from TFY3301-RR decreased by 89.03 and 91.77% relative to MC and $LR_1$. The TFY3301-RR system showed

**Table 3 $^{13}C$ Labeling of MC, RSR and $LR_1$ with RSR synchronous heading (mg/plant)**

| Variety (V)[1)] | Cultivation pattern (C)[2)] | $^{13}C$-soil | $^{13}C$-root | $^{13}C$-stem | $^{13}C$-leaf | $^{13}C$-grain |
|---|---|---|---|---|---|---|
| TFY3301 | MC | 17.5 a | 43.85 a | 114.27 a | 42.78 b | 241.35 bc |
| | RSR | 3.2 c | 26.53 c | 45.53 c | 28.76 c | 282.76 a |
| | $LR_1$ | 16.8 a | 44.86 a | 98.24 a | 42.88 b | 250.34 b |
| NL1 | MC | 11.3 b | 38.42 b | 74.68 b | 54.25 a | 197.34 c |
| | RSR | 5.4 c | 25.52 c | 22.56 d | 32.71 c | 212.71 cd |
| | $LR_1$ | 12.6 b | 37.83 b | 78.21 cd | 48.83 ab | 202.34 d |
| *F*-value | V | 10.228** | NS | 59.919*** | 9.539** | 49.633*** |
| | C | 64.058*** | 17.367*** | 43.631*** | 23.057*** | 4.962* |
| | V×C | 8.797** | NS | 4.183* | NS | NS |

[1)] TFY3301 and NL1 refer to the hybrid rice variety Taifengyou 3301 and the conventional variety Nanling 1, respectively.
[2)] MC, main crop rice; RSR, ratoon season rice; $LR_1$, single-cropping mid-late rice synchronized in heading time with RSR.
Different lowercase letters within the same column indicate significant differences (ANOVA, $P<0.05$). NS indicates no significant difference at the 0.05 probability level; ***, **, and * denote significant differences at the 0.001, 0.01, and 0.05 probability levels, respectively.

$CH_4$ reductions of 16.80 and 36.15% compared to $LR_1$ and DC, respectively. Similarly, NL1-RSR resulted in 89.19 and 90.36% lower $CH_4$ emissions compared to MC and $LR_1$. The NL1-RR system exhibited declines of 1.22 and 48.90% relative to $LR_1$ and DC, respectively.

In 2021, the annual cumulative $N_2O$ emissions from TFY3301-RSR were reduced by 48.90 and 47.71% compared to its MC and $LR_1$ counterparts, respectively. The TFY3301-RR system emitted 54.63 and 20.47% more $N_2O$ than $LR_1$ and DC, respectively. For NL1-RSR, $N_2O$ emissions decreased by 43.29 and 37.26% relative to MC and $LR_1$. In contrast, the NL1-RR system showed a 73.37% increase in $N_2O$ emissions compared to $LR_1$, but a 14.45% reduction relative to DC. In 2022, TFY3301-RSR reduced cumulative $N_2O$ emissions by 46.00 and 41.67% compared to MC and $LR_1$, respectively. The TFY3301-RR system had 66.33 and 3.93% higher $N_2O$ emissions than $LR_1$ and DC, respectively. For NL1-RSR, $N_2O$ emissions were reduced by 33.23 and 15.11% relative to MC and $LR_1$. Meanwhile, the NL1-RR system exhibited a substantial 112.04% increase in $N_2O$ emissions compared to $LR_1$, yet still showed an 8.59% reduction relative to DC.

In 2021, the $CO_2$ emission flux for RSR ranged from 0.01 to 0.56 g $m^{-2}$ $h^{-1}$, with an average reduction of 33.33 to 39.35% compared to MC and $LR_1$. Across both years, the $CH_4$ emission fluxes for MC and $LR_1$ peaked at 8.64 to 17.53 mg $m^{-2}$ $h^{-1}$, whereas the peak $CH_4$ emission flux for RSR occurred during the tillering stage, ranging from 0.87 to 2.63 mg $m^{-2}$ $h^{-1}$. Notably, $CH_4$ emissions from RSR were higher during the tillering stage than during the heading stage — a trend distinct from that observed in MC and $LR_1$. The $N_2O$ emission fluxes for MC and $LR_1$ were detected within a few days following fertilization. In contrast, the peak $N_2O$ emission flux for RSR occurred during the tillering stage and the grain fertilizer application period 3 days after harvest, ranging from 6.25 to 178.06 μg $m^{-2}$ $h^{-1}$, compared to 2.49 to 275.12 μg $m^{-2}$ $h^{-1}$ for MC and $LR_1$. The $CO_2$, $CH_4$, and $N_2O$ emission fluxes under the DC pattern were comparable to those of MC and $LR_1$, as shown in Fig. 1.

### 3.4. Analysis of daily average cumulative GHG emissions

Due to differences in full growth durations among varieties, daily average emissions of $CO_2$, $CH_4$, and $N_2O$ were used for quantification. As shown in Fig. 2, in 2021, the daily $CO_2$ emissions of TFY3301-RSR were 11.93 and 0.68% lower than those of its MC and $LR_1$, respectively; TFY3301-RR emitted 4.36% less than TFY3301-MC but 7.85% more than $LR_1$. NL1-RSR emissions were 36.53 and 32.42% lower than those of its MC and $LR_1$, respectively; NL1-RR was 14.42 and 8.87% lower than its MC and $LR_1$. In 2022, TFY3301-RSR emissions were 10.85% higher than MC but 12.48% lower than $LR_1$; the TFY3301-RR emitted 3.97% more than MC but 17.91% less than $LR_1$. NL1-RSR emissions were 26.82 and 26.11% lower than its MC and $LR_1$, respectively; NL1-RR was 10.59 and 9.72% lower than its MC and $LR_1$.

In 2021, the daily cumulative $CH_4$ emissions from TFY3301-RSR were reduced by 91.78 and 90.60% compared to its MC and $LR_1$, respectively. Similarly, TFY3301-RR showed reductions of 33.58 and 24.06% relative to its MC and $LR_1$. For NL1-RSR, emissions decreased by 81.76 and 83.87% compared to its MC and $LR_1$, while NL1-RR exhibited decreases of 32.27 and 40.12% relative to its MC and $LR_1$. In 2022, TFY3301-RSR demonstrated reductions of 80.98 and 85.74% compared to its MC and $LR_1$, respectively. TFY3301-RR also showed significant decreases of 29.63 and 47.24% relative to its MC and $LR_1$. NL1-RSR and NL1-RR displayed reductions of 83.42 and 85.22%, and 32.93 and 40.21%, respectively, compared to their corresponding MC and $LR_1$ values. Furthermore, analysis revealed that daily $N_2O$ emissions among RSR, MC, and $LR_1$ varied minimally, indicating negligible differences in $N_2O$ output across these cropping systems.

In 2021, the daily cumulative $CH_4$ emissions from the RR systems TFY3301-RR and NL1-RR were 9.65 and 23.54% lower, respectively, than those of the DC system comprising JFZ in the early rice season and YY2640 in the late rice season. In 2022, the reductions reached 25.55 and 35.71%, respectively. No significant differences were observed in daily cumulative $CO_2$ or $N_2O$ emissions between the systems.

### 3.5. Analysis of daily GWP and GHG intensity

As illustrated in Fig. 3, in 2021, the daily average GWP of TFY3301 RSR was reduced by 83.12 and 80.94% compared to its MC and genetically identical $LR_1$, respectively. Similarly, TFY3301-RR showed reductions of 30.41 and 21.43% relative to its MC and $LR_1$, respectively. For NL1, the daily average GWP of its RSR decreased by 74.80 and 77.26% compared to its MC and $LR_1$, respectively, while its RR pattern exhibited reductions of 29.53 and 36.40% relative to its MC and $LR_1$, respectively. In 2022, the daily average GWP of TFY3301-RSR declined by 72.84 and 78.93% compared to its MC and $LR_1$, respectively. The TFY3301-RR pattern also demonstrated reductions of 26.65 and 43.11% relative to its MC and $LR_1$, respectively. For NL1, the daily average GWP of its RSR

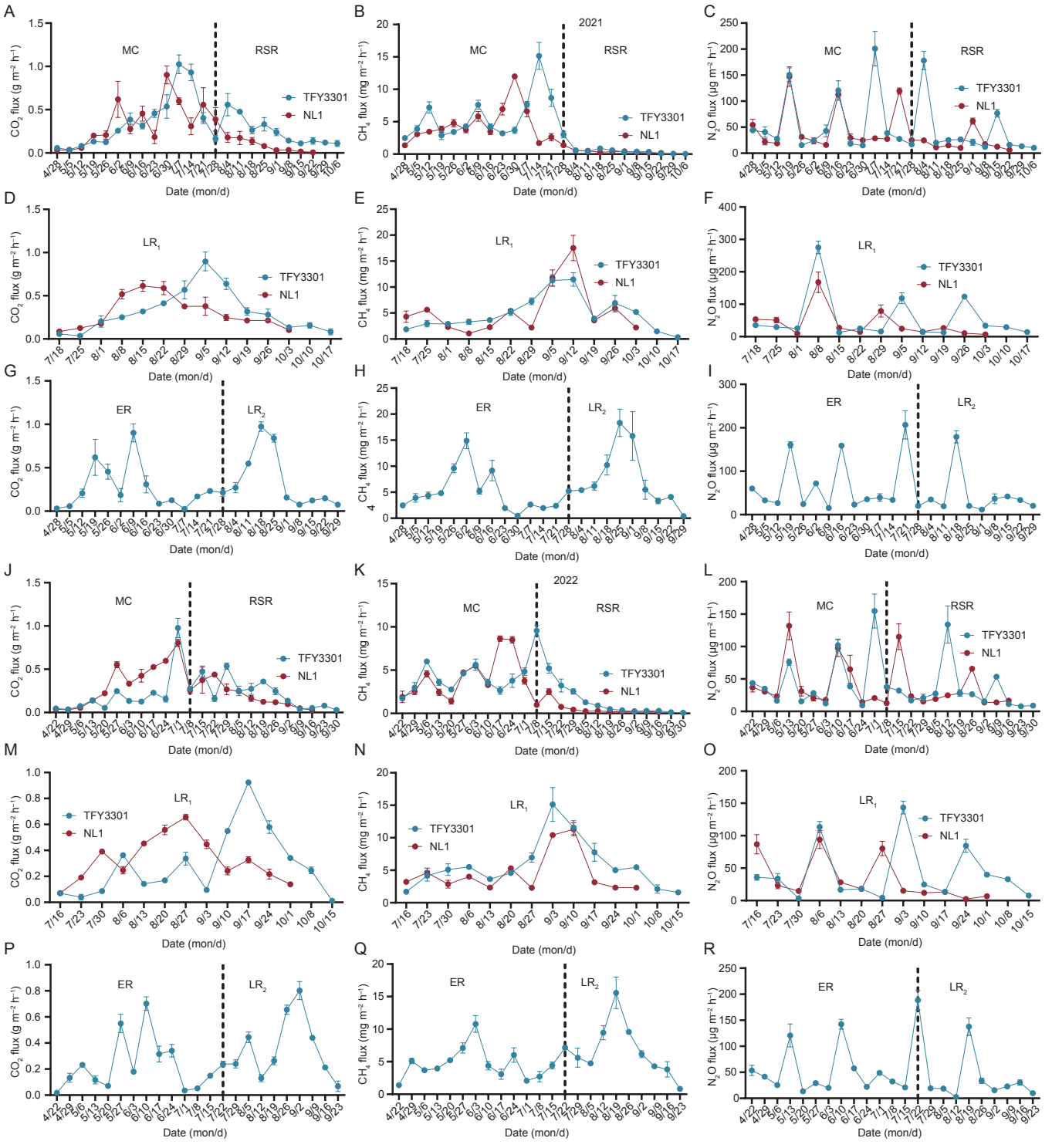



**Fig. 1 Greenhouse gas emission fluxes from MC, RSR, $LR_1$, and DC in 2021 and 2022.** TFY3301 and NL1 refer to the hybrid rice variety Taifengyou 3301 and the conventional variety Nanling 1, respectively. MC, main crop rice; RSR, ratoon season rice; $LR_1$, single-season mid-late rice with synchronized heading relative to RSR; DC, double-cropping rice; ER, double-cropping early rice; $LR_2$, double-cropping late rice. Error bars represent SD ($n$=3).

decreased by 73.94 and 75.98% compared to its MC and $LR_1$, respectively, while its RR pattern showed decreases of 29.19 and 34.72% relative to its MC and $LR_1$, respectively.

In 2021, TFY3301-RSR exhibited a 77.33 and 74.35% reduction in daily GHGI relative to its MC and $LR_1$, respectively. The TFY3301-RR pattern showed a 60.11 and 54.87% decrease compared to its MC and $LR_1$, respectively. For NL1, the daily GHGI of RSR was reduced by 72.95 and 72.80% in comparison to its MC and $LR_1$, while its RR pattern decreased by 63.51 and 63.32%, respectively. In 2022, TFY3301-RSR demonstrated a 65.13 and 72.12% decline in daily GHGI compared to its MC and $LR_1$, respectively. The

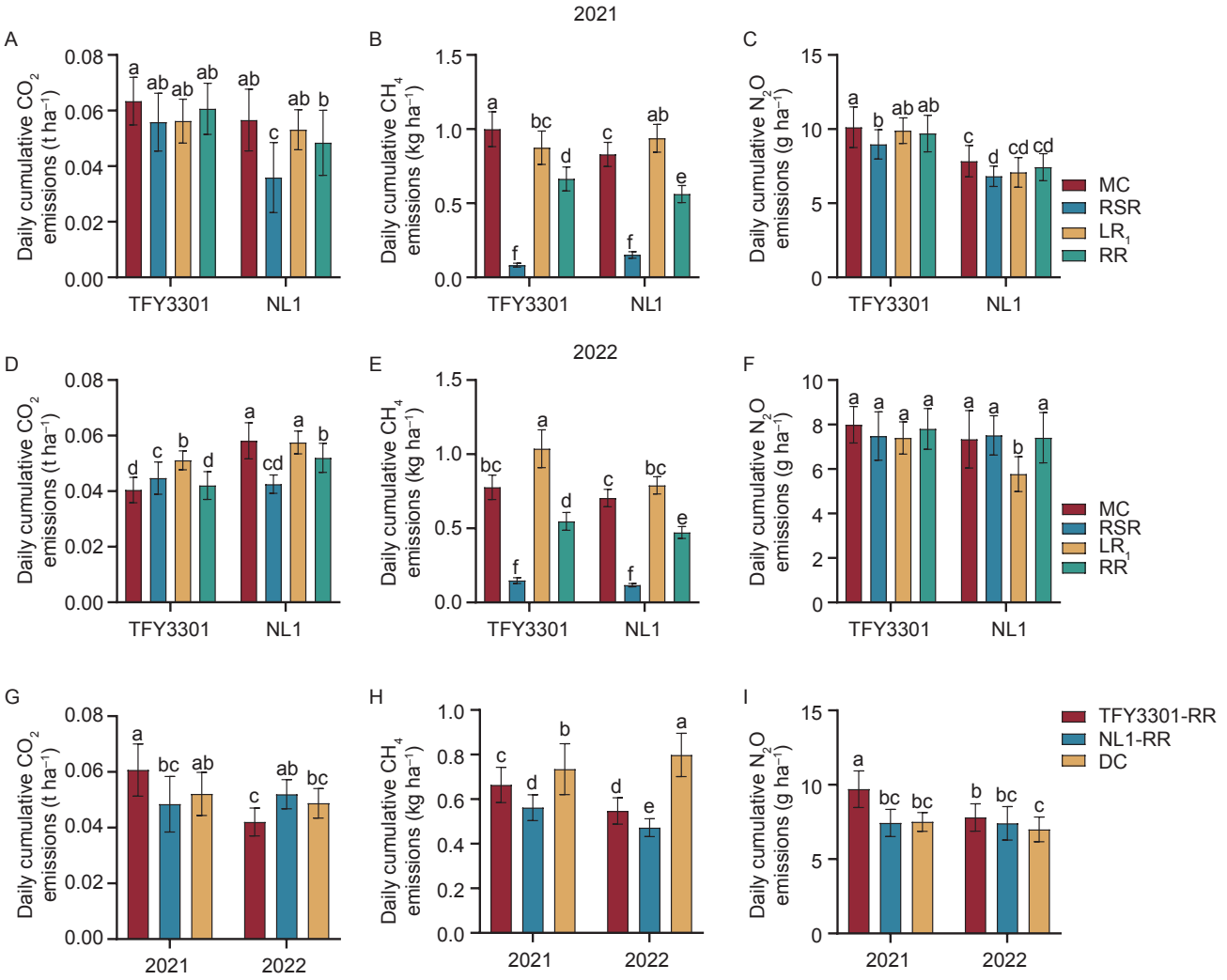



**Fig. 2 Daily average greenhouse gas emissions of MC, RSR, $LR_1$, RR, and DC in 2021 and 2022.** TFY3301 and NL1 refer to the hybrid rice variety Taifengyou 3301 and the conventional variety Nanling 1, respectively. MC, main crop rice; RSR, ratoon season rice; $LR_1$, single-season mid-late rice with synchronized heading relative to RSR; RR, ratooning rice; DC, double cropping rice. Error bars represent SD ($n$=3). Different lowercase letters indicate significant differences (ANOVA, $P$<0.05).

RR pattern of TFY3301 was reduced by 58.77 and 67.03% relative to its MC and $LR_1$. Similarly, NL1-RSR showed a reduction in daily GHGI by 72.89 and 72.31% compared to its MC and $LR_1$, while its RR pattern decreased by 63.90 and 63.12%, respectively.

In 2021, the cumulative daily GWP of the RR pattern for TFY3301 and NL1 decreased by 5.42 and 21.08%, respectively, compared with the DC pattern. In 2022, the reductions were 27.41 and 36.42%, respectively. Similarly, in 2021, the cumulative daily GHGI of the RR pattern for TFY3301 and NL1 showed a reduction of 18.71 and 19.49%, respectively, compared with the DC pattern. In 2022, the reductions were 39.02 and 37.15%, respectively.

As illustrated in Fig. 4, the $CO_2$ emission intensity of TFY3301-RSR in 2021 was 31.79 and 22.89% lower than that of its MC and $LR_1$, respectively. The TFY3301-RR system achieved modest reductions of 2.32 and 6.85% relative to $LR_1$ and DC, respectively. For the NL1 variety, RSR resulted in substantial declines of 55.56 and 47.29% compared to MC and $LR_1$, respectively. Furthermore, the NL1-RR system demonstrated reductions of 13.16 and 18.15% relative to $LR_1$ and DC, respectively. In 2022, TFY3301-RSR exhibited $CO_2$ emission intensity reductions of 17.19 and 33.18% compared to MC and $LR_1$, respectively. The TFY3301-RR system demonstrated reductions of 24.99 and 32.62% relative to $LR_1$ and DC. For the NL1 cultivar, RSR declined by 50.35 and 44.46% compared to MC and $LR_1$, respectively. The NL1-RR system achieved reductions of 15.74 and 9.01% relative to $LR_1$ and DC.

In 2021, the TFY3301-RSR led to substantial reductions in $CH_4$ emission intensity, by 93.63 and 92.70% compared to its MC and $LR_1$, respectively. The TFY3301-RR demonstrated declines of 31.22 and 27.64% relative to $LR_1$ and DC. The NL1-RSR resulted in reductions of 87.23 and 87.42% compared with its MC and $LR_1$ counterparts, respectively. Likewise, the NL1-RR exhibited reductions of 42.94 and 32.63% relative to $LR_1$ and DC, respectively. Consistent with this trend, in 2022, $CH_4$ emission intensity under the TFY3301-

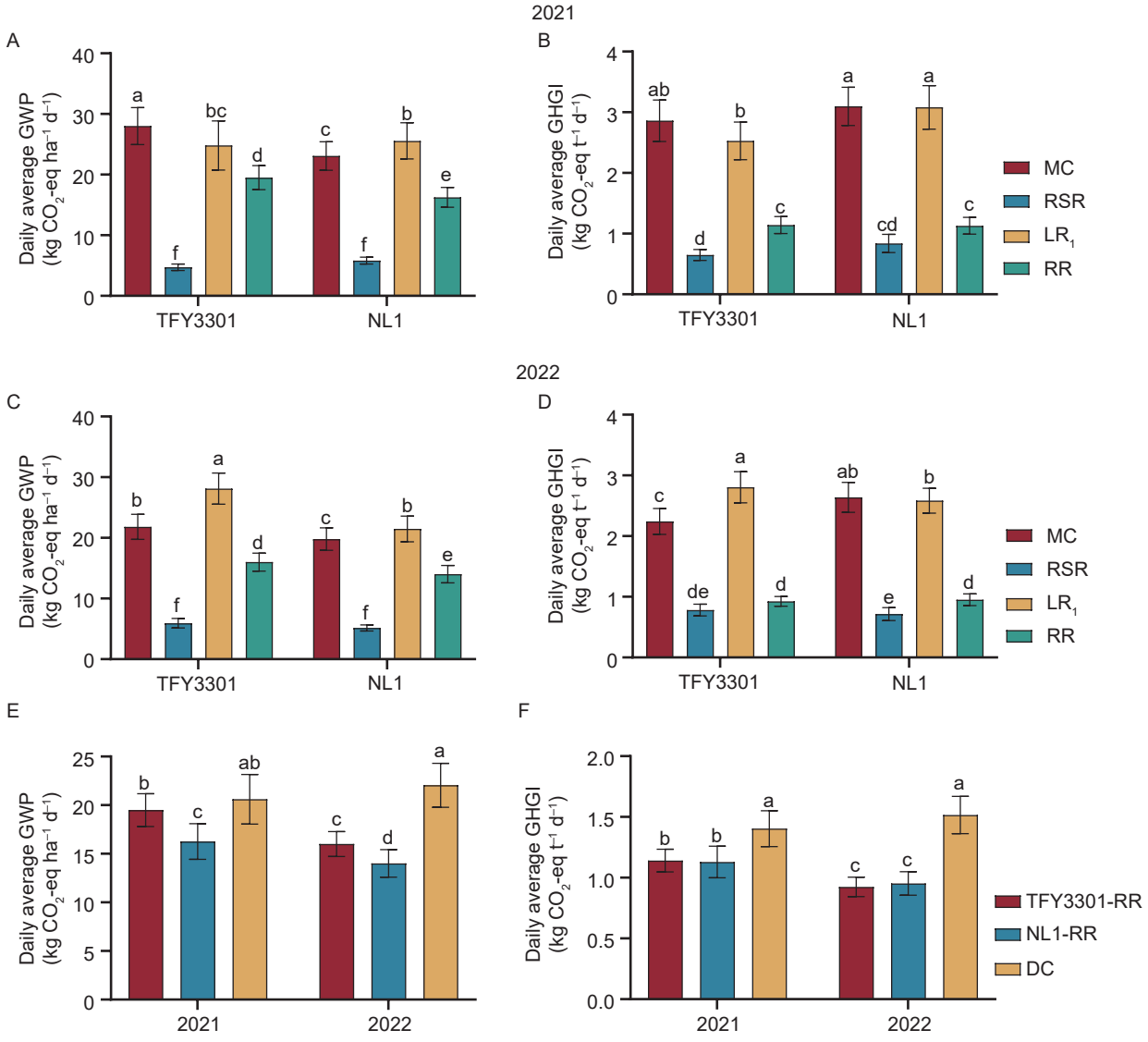



**Fig. 3 Global warming potential and greenhouse gas intensity of MC, RSR, $LR_1$, RR, and DC in 2021 and 2022.** TFY3301 and NL1 refer to the hybrid rice variety Taifengyou 3301 and the conventional variety Nanling 1, respectively. MC, main crop rice; RSR, ratoon season rice; $LR_1$, single-season mid-late rice with synchronized heading relative to RSR; RR, ratooning rice; DC, double cropping rice. GWP, global warming potential; GHGI, greenhouse gas intensity. Error bars represent SD ($n$=3). Different lowercase letters indicate significant differences (ANOVA, $P$<0.05).

RSR decreased by 85.92 and 89.11% compared to its MC and $LR_1$, respectively. The TFY3301-RR achieved reductions of 51.79 and 46.36% relative to $LR_1$ and DC. For NL1-RSR, $CH_4$ emission intensity decreased by 88.75 and 88.89% compared with MC and $LR_1$, respectively. The NL1-RR yielded reductions of 44.19 and 49.49% relative to $LR_1$ and DC.

In 2021, the TFY3301-RSR reduced $N_2O$ emission intensity by 31.38 and 29.63% relative to its MC and $LR_1$, respectively. The TFY3301-RR achieved an 11.19% reduction compared to $LR_1$, though it exhibited a slight increase of 3.54% relative to DC. The NL1-RSR lowered $N_2O$ emission intensity by 39.13 and 24.97% compared with MC and $LR_1$, respectively. The NL1-RR system showed negligible difference from $LR_1$ but attained a 12.73% reduction when compared to DC. In 2022, the $N_2O$ emission intensity under the TFY3301-RSR declined by 30.68 and 22.82% compared to its MC and $LR_1$, respectively. The TFY3301-RR demonstrated reductions of 3.62 and 12.71% relative to $LR_1$ and DC. For NL1, the RSR resulted in reductions of 30.55 and 2.15% compared to MC and $LR_1$, respectively. However, the RR system for NL1 exhibited a 19.79% increase relative to $LR_1$, while still achieving a 9.64% reduction compared with DC.

### 3.6. Analysis of carbon and nitrogen footprints

As illustrated in Fig. 5, in 2021, the TFY3301-RSR in the RR system exhibited a significantly reduced carbon footprint compared to its MC and the $LR_1$, with reductions of 77.70 and 76.08%, respectively. Conversely, the carbon footprint of the RR system increased by 22.30 and 31.19% relative to MC and $LR_1$. Similarly, the NL1-RSR in the NL1 RR system showed reductions of 71.34 and 72.88% compared to its MC and the $LR_1$, while the NL1-RR increased by 28.66 and 21.76%. In

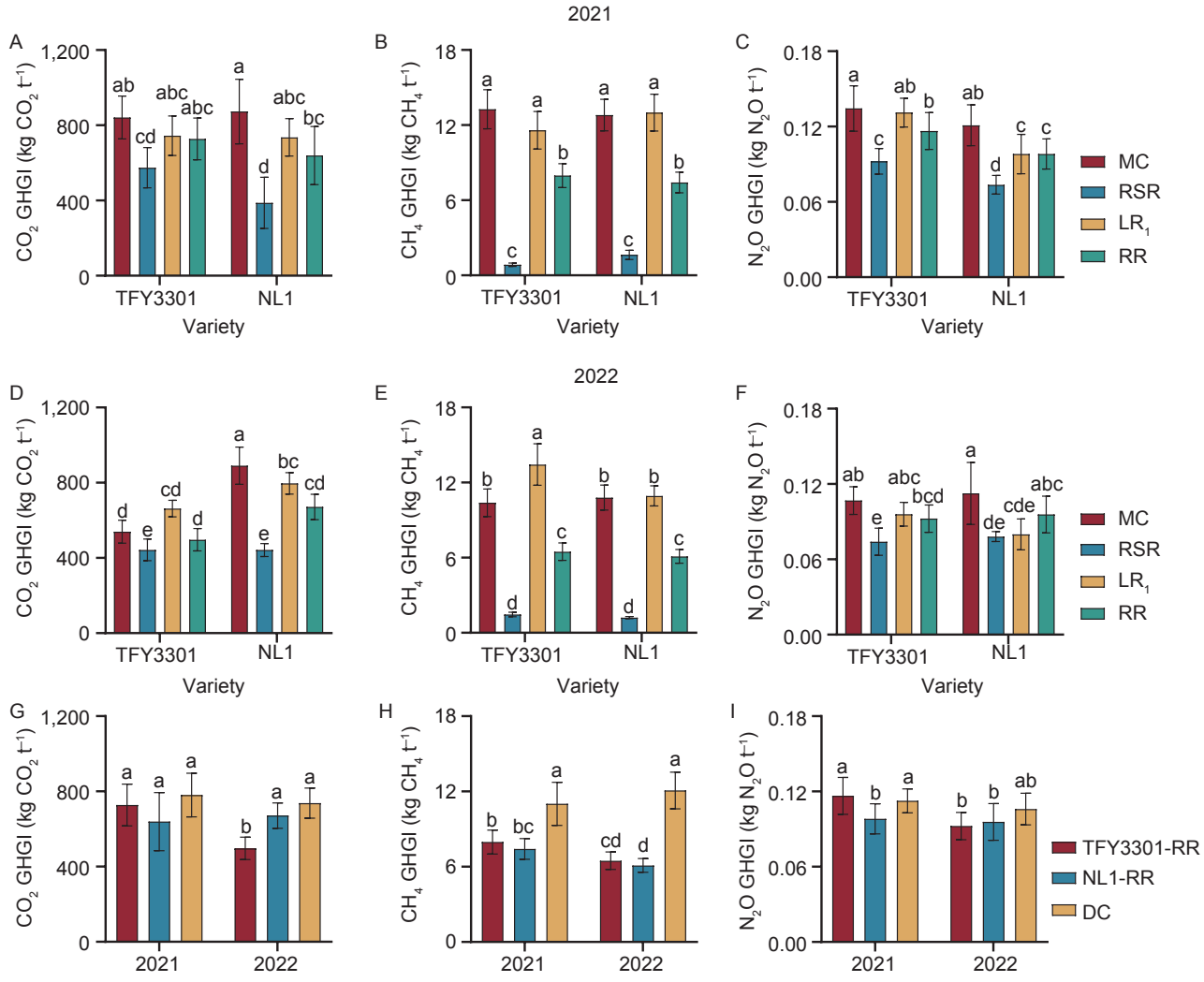



**Fig. 4 $CO_2$, $CH_4$, and $N_2O$ emission intensity of MC, RSR, $LR_1$, RR, and DC in 2021 and 2022.** TFY3301 and NL1 refer to the hybrid rice variety Taifengyou 3301 and the conventional variety Nanling 1, respectively. MC, main crop rice; RSR, ratoon season rice; $LR_1$, single-season mid-late rice with synchronized heading relative to RSR; RR, ratooning rice; DC, double cropping rice. GHGI, greenhouse gas intensity. Different lowercase letters indicate significant differences (ANOVA, $P$<0.05). Bars represent SD ($n$=3).

2022, the carbon footprint of TFY3301-RSR decreased by 72.26 and 75.85% compared to MC and $LR_1$, whereas the TFY3301-RR increased by 27.74 and 11.19% relative to MC and $LR_1$. Additionally, the NL1-RSR demonstrated reductions of 69.28 and 70.47%, while the NL1-RR increased by 30.72 and 25.66% compared to MC and $LR_1$.

In terms of nitrogen footprint, in 2021, TFY3301-RSR exhibited a reduction of 29.52 and 36.52% compared to its MC and the $LR_1$, respectively. The RR system of TFY3301 showed an increase of 70.48 and 53.55% compared to MC and $LR_1$, respectively. For the NL1-RSR, there was a reduction of 27.08 and 34.51% compared to its MC (early season) and the $LR_1$ (late season), respectively. Additionally, the nitrogen footprint of NL1-RR increased by 72.92 and 55.31% compared to MC (early season) and $LR_1$ (late season), respectively. In 2022, consistent results were observed: TFY3301-RSR nitrogen footprint decreased by 29.46 and 36.42% compared to MC and $LR_1$, respectively, while the TFY3301-RR footprint increased by 70.54 and 53.71% compared to its MC and $LR_1$, respectively. Similarly, the NL1-RSR nitrogen footprint was reduced by 26.89 and 34.20% compared to MC and $LR_1$, respectively, and the NL1-RR system footprint increased by 73.11 and 55.80% compared to NL1-MC and NL1-$LR_1$, respectively.

In the context of the DC pattern, the carbon footprint of the TFY3301-RR and NL1-RR patterns decreased by 19.13 and 29.87%, and by 28.22 and 36.17% compared to the DC pattern in 2021 and 2022, respectively. Similarly, the nitrogen footprint for the RR pattern of TFY3301 and NL1 was reduced by 19.56–21.53% and 19.80–21.45% relative to that of the DC pattern in 2021 and 2022.

### 3.7. Analysis of resource use efficiency and daily average economic benefits

As illustrated in Fig. 6, in 2021, the resource use efficiency of TFY3301-RSR increased by 87.50 and 87.11% relative to its MC and $LR_1$, respectively. The TFY3301-RR system also showed improvements of 24.87 and 24.62% compared to MC and $LR_1$. For NL1-RSR, efficiency rose by 127.44 and 104.15% relative to MC and $LR_1$, while the NL1-RR system

demonstrated gains of 37.03 and 23.00%, respectively. In 2022, TFY3301-RSR efficiency increased by 96.05 and 90.19% compared to MC and $LR_1$, and the corresponding RR system achieved enhancements of 27.31 and 23.51%. Similarly, NL1-RSR showed improvements of 128.16 and 105.92% relative to MC and $LR_1$, with its RR system increasing by 37.99 and 24.54% over the same benchmarks.

In 2021, the daily economic benefits of TFY3301-RSR increased significantly by 101.06 and 99.56% relative to its MC and $LR_1$, respectively. The daily economic benefits of TFY3301-RR improved by 36.97 and 35.95% compared to MC and $LR_1$. Additionally, the daily economic benefits of NL1-RSR rose by 149.65 and 99.13% relative to MC and $LR_1$, while the RR system exhibited enhancements of 59.07 and 26.88% over these controls. In 2022, TFY3301-RSR continued to show higher performance, with daily economic benefits increasing by 118.54 and 108.81% relative to MC and $LR_1$. The RR system also improved by 43.37 and 35.67%. Furthermore, NL1-RSR displayed substantial gains of 165.73 and 112.55% relative to MC and $LR_1$, while the NL1 system improved by 65.42 and 32.31% compared to the respective controls.

In 2021, the daily resource use efficiency of RR varieties TFY3301 and NL1 increased by 57.53 and 35.66%, respectively, relative to the DC variety. In 2022, these values were 57.37 and 39.42%, respectively. Similarly, daily

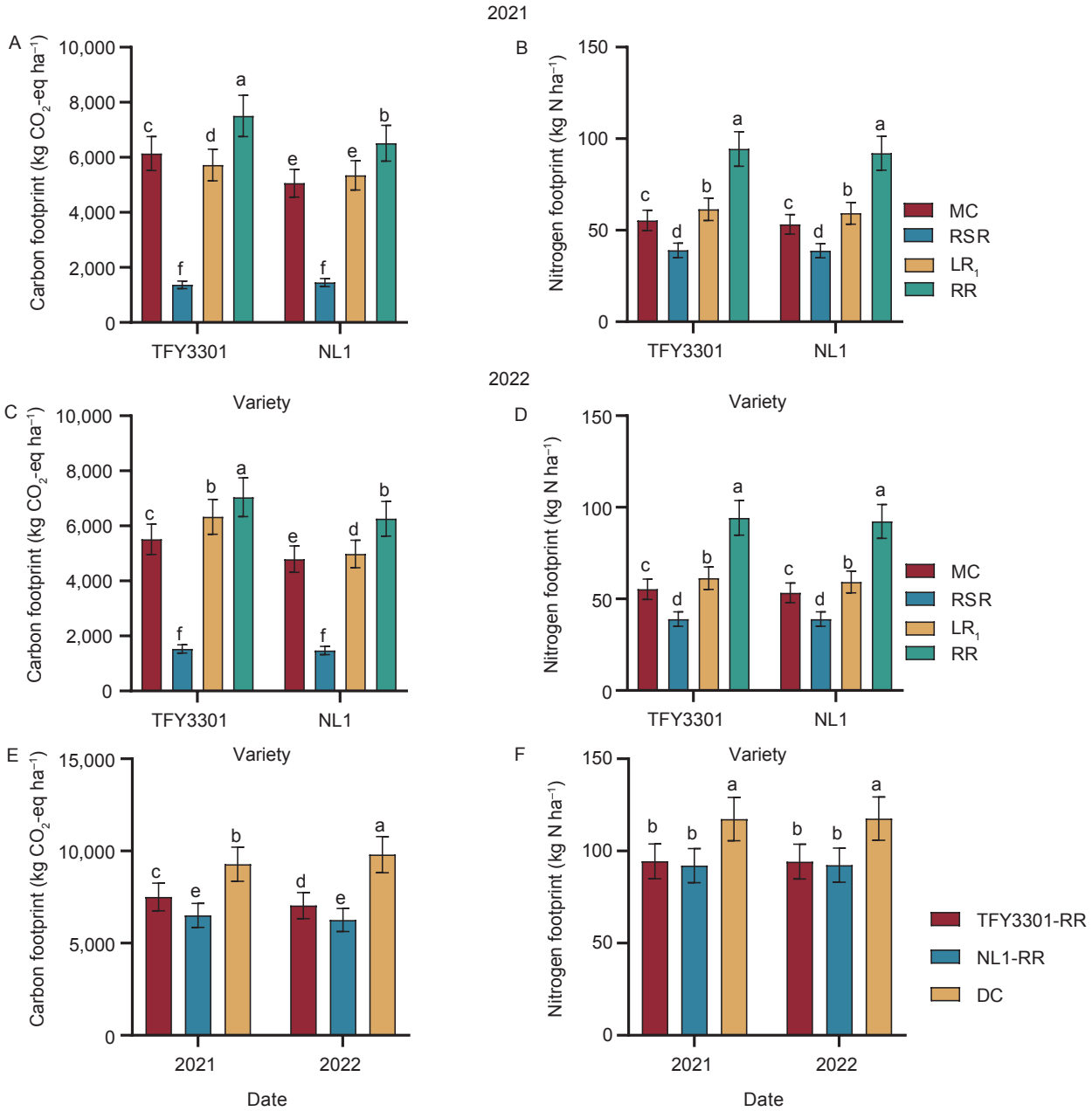



**Fig. 5 Carbon footprint and nitrogen footprint of MC, RSR, $LR_1$, RR, and DC in 2021 and 2022.** TFY3301 and NL1 refer to the hybrid rice variety Taifengyou 3301 and the conventional variety Nanling 1, respectively. MC, main crop rice; RSR, ratoon season rice; $LR_1$, single-season mid-late rice with synchronized heading relative to RSR; RR, ratooning rice; DC, double cropping rice. Bars represent SD ($n$=3). Different lowercase letters indicate significant differences (ANOVA, $P$<0.05).

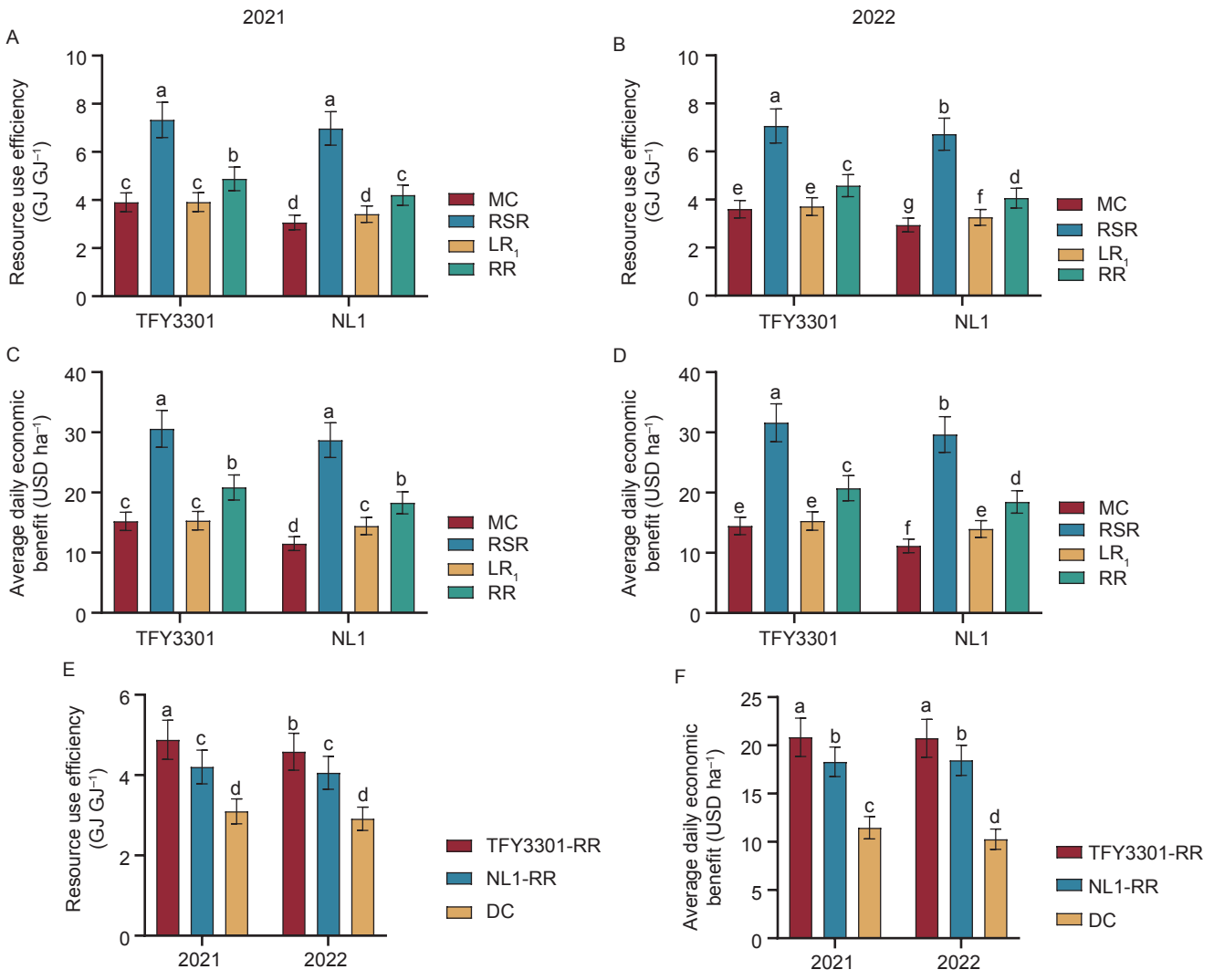



**Fig. 6 Energy use efficiency and daily economic benefits of MC, RSR, $LR_1$, RR, and DC in 2021 and 2022.** TFY3301 and NL1 refer to the hybrid rice variety Taifengyou 3301 and the conventional variety Nanling 1, respectively. MC, main crop rice; RSR, ratoon season rice; $LR_1$, single-season mid-late rice with synchronized heading relative to RSR; RR, ratooning rice; DC, double cropping rice. Bars represent SD ($n$=3). Different lowercase letters indicate significant differences (ANOVA, $P$<0.05).

economic benefits for TFY3301 and NL1 increased by 81.85 and 59.61% in 2021, and by 101.86 and 79.66% in 2022 relative to DC. These results indicate that the performance trends of different planting patterns remained consistent across both years.

### 3.8. Analysis of carbon sequestration capacity and carbon balance

The carbon budget balance was determined by assessing the carbon sequestration (fixation) capacity of plants relative to their carbon emissions. As illustrated in Fig. 7, in 2021, the carbon sequestration capacity of TFY3301-RSR decreased by 34.04 and 36.69% compared to TFY3301-MC and TFY3301-$LR_1$, respectively, whereas TFY3301-RR increased by 65.96 and 59.29% relative to MC and $LR_1$. Similarly, the carbon sequestration capacity of NL1-RSR declined by 21.76 and 25.15% compared to NL1-MC and NL1-$LR_1$, while NL1-RR increased by 78.24 and 70.52% relative to the corresponding MC and $LR_1$ systems. In 2022, TFY3301-RSR exhibited a reduction of 31.17 and 33.69% compared to its MC and $LR_1$ counterparts, whereas the RR system showed increases of 68.83 and 62.66% relative to MC (early season) and $LR_1$ (late season), respectively. Likewise, NL1-RSR decreased by 15.45 and 18.05% compared to MC and $LR_1$; in contrast, NL1-RR increased by 84.55 and 78.87% relative to the respective counterparts.

In 2021, direct and indirect GHG emissions from TFY3301-RSR and NL1-RSR were significantly lower — by 56.88–65.84% — compared to the corresponding MC and $LR_1$ genotypes. Conversely, the two RR systems showed increases of 34.16–55.93% in emissions relative to their MC and $LR_1$ counterparts.

In 2021, the carbon budget surplus of TFY3301-RSR increased by 2.28% relative to TFY3301-MC; the TFY3301-RR system exhibited increases of 102.28 and 65.50% compared to TFY3301-MC and TFY3301-$LR_1$, respectively. NL1-RSR also demonstrated a rise in carbon budget surplus of 37.30

and 22.44% relative to NL1-MC and NL1-$LR_1$; the NL1-RR system showed increases of 137.30 and 111.62% compared to MC and $LR_1$, respectively. A similar trend was observed in 2022: the TFY3301-RR system increased by 85.95 and 103.23% relative to TFY3301-MC and TFY3301-$LR_1$. NL1-RSR showed increases of 44.43 and 36.29% in carbon budget surplus relative to MC and $LR_1$; the NL1-RR system further increased by 144.43 and 130.65% compared to the respective counterparts.

In 2021, the carbon sequestration capacity of RR varieties TFY3301 and NL1 was lower than that of the DC. Indirect emissions from TFY3301 and NL1 decreased by 26.06 and 27.98%, respectively, compared to the DC system. This trend persisted in 2022, with reductions of 24.17 and 27.44% in indirect emissions. Direct emissions from TFY3301 showed minimal difference compared to the DC system, while NL1 exhibited a 23.19% reduction in 2021. In 2022, direct emissions from TFY3301 and NL1 decreased by 23.70 and 19.51%, respectively, relative to the DC system. Furthermore, the $LR_1$ carbon budget surplus ranged from 8,917.65 to 13,469.85 kg $CO_2$-eq $ha^{-1}$, whereas those of the RR and DC systems ranged from 19,704.37 to 27,375.09 kg $CO_2$-eq $ha^{-1}$ and 23,199.78 to 24,344.52 kg $CO_2$-eq $ha^{-1}$, respectively.

These results collectively demonstrate that RR exhibits superior carbon sink capacity, lower carbon-nitrogen footprints, and higher carbon fixation, GHG emission reduction, and resource use efficiency compared to both $LR_1$ and DC systems. These advantages are primarily attributed to the enhanced allocation of photosynthetic assimilates to panicles and reduced allocation to the soil ecosystem during the RSR cycle, resulting in lower GHG emissions, increased economic coefficient, and higher daily average yield.

## 4. Discussion

### 4.1. Physiological mechanisms underlying yield and GHG emission dynamics of RR

In China, rice serves not only as a staple food crop but also as a major source of GHG emissions. The “Global Methane Pledge” aims to reduce agricultural $CH_4$ emissions by over 30% by 2030, with a significant proportion originating from

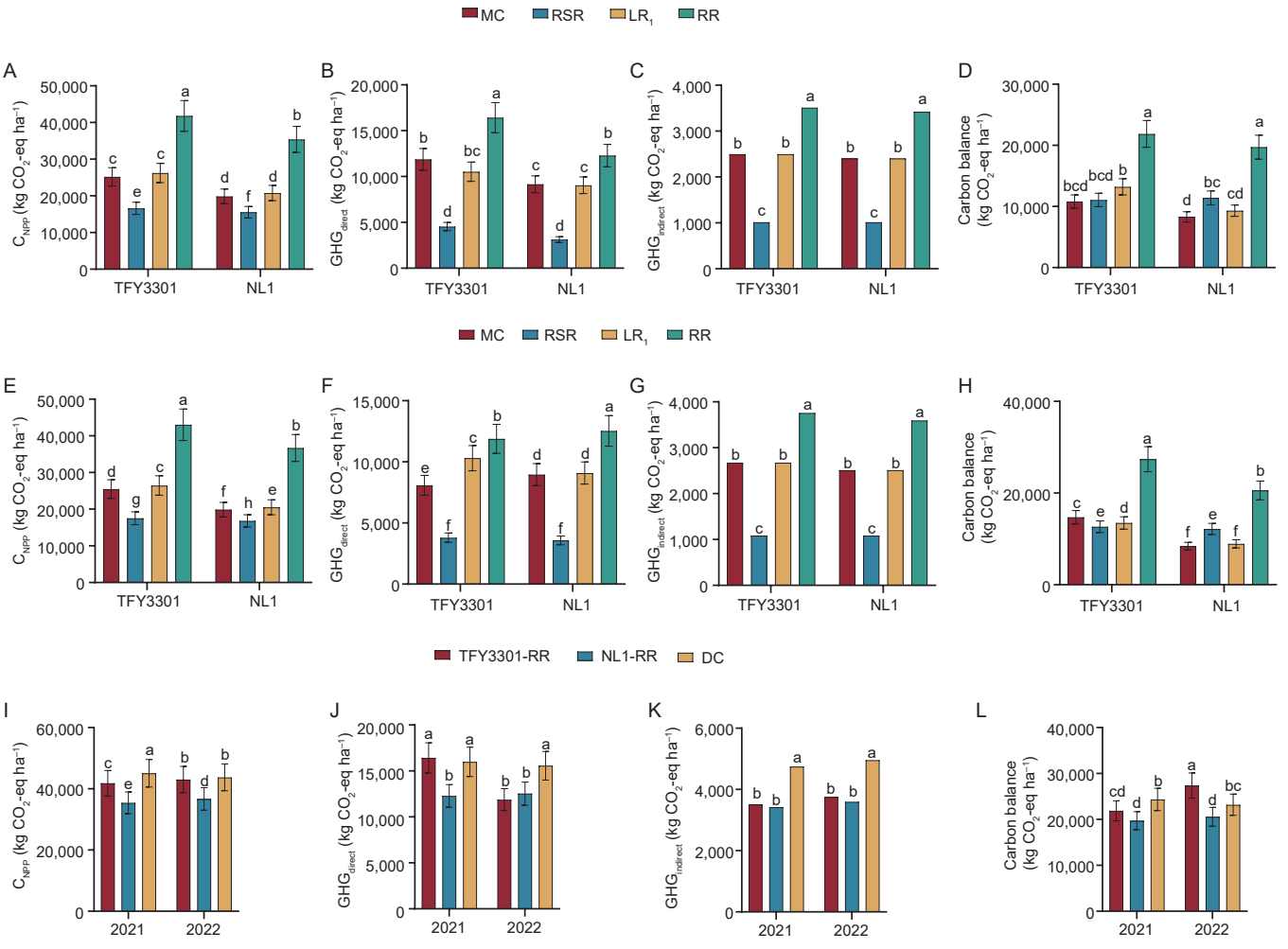



**Fig. 7 Carbon sequestration and carbon balance of MC, RSR, $LR_1$, RR, and DC in 2021 and 2022.** TFY3301 and NL1 refer to the hybrid rice variety Taifengyou 3301 and the conventional variety Nanling 1, respectively. MC, main crop rice; RSR, ratoon season rice; $LR_1$, single-season mid-late rice with synchronized heading relative to RSR; RR, ratooning rice; DC, double cropping rice. $C_{NPP}$, the $CO_2$ fixation associated with net primary productivity; $GHG_{direct}$, the carbon dioxide equivalent of direct greenhouse gas emissions; $GHG_{indirect}$, greenhouse gas. Error bars represent SD ($n$=3). Different lowercase letters indicate significant differences (ANOVA, $P$<0.05).

rice paddy fields (Huang *et al.* 2022). Therefore, enhancing the capacity of rice paddies to sequester carbon and mitigate $CH_4$ emissions — while ensuring sustained increases in yield — is critical for environmental security. Rice cultivation practices such as variety selection, water and nutrient management, and cropping patterns can simultaneously improve productivity and reduce carbon emissions. Currently, rice ratooning is gaining adoption in southern China. Over the past two decades, RSR yields have increased from 3,000 kg $ha^{-1}$ to a maximum of 9,000 kg $ha^{-1}$, improving farmer income and expanding cultivated area. We conducted a two-year field study in southeastern China using varieties with distinct genetic traits to evaluate their effects on GHG emissions and yield performance, while assessing changes in carbon accumulation and carbon budget balance (Yuan *et al.* 2019; Song *et al.* 2021; Yu *et al.* 2021; Xu *et al.* 2022). In this study, the daily yield of RSR under the RR system was 28.21–47.40% higher than that of its MC and $LR_1$ (Table 1; Appendix C). This enhancement in daily yield during the ratoon season arises primarily from the activation of axillary buds at multiple nodes on residual stubble following harvest of the MC. These dormant buds differentiate into productive tillers, resulting in a 31.71–50.38% increase in effective panicles during the ratoon season. The panicle quantity compensation mechanism effectively offsets the reduced grain number per panicle commonly observed in ratoon crops, particularly under mechanical harvesting with low stubble height (15–25 cm), demonstrating notable biological plasticity in yield component regulation. Notably, removal of apical dominance in low-stubble treatments stimulates development of the 1st and 2nd nodal buds, which contribute more than 80% of total productive tillers. The physiological basis for this response includes enhanced root activity and optimized nitrogen allocation through split fertilization, collectively improving photosynthate translocation efficiency during the critical panicle formation stage. Consequently, the production efficiency of RSR — measured as daily yield — is significantly greater than that of MC and $LR_1$ (where MC and $LR_1$ represent early-season and late-season single crops, respectively, used for comparison with RSR). Both RR systems with differing maturity periods achieved total yield increases of 13.50–27.76% compared to the traditional DC system.

Further analysis revealed that $CO_2$ and $CH_4$ emissions from the RR system during the regrowth season were substantially lower. Cumulative $CH_4$ emissions from various RSR types — maturing in the late season — decreased by over 70% compared to those from their corresponding MC (matured in the early season) and $LR_1$ (serving as a synchronous-heading control matured in the late season). The former comparison (RSR *vs*. MC) involved the same genotype across seasons, whereas the latter (RSR *vs*. $LR_1$) compared the same genotype within the same season under different cultivation methods (ratooning versus seedling transplanting). These results align with previous findings indicating that the RR system exhibits lower GHG emissions than other rice cropping systems, primarily because RSR reduces daily cumulative field emissions (Chen *et al.* 2019; Liu 2019; Shi *et al*. 2020). Quantification of emissions showed that average daily cumulative $CH_4$ emissions from RSR declined by 80.98–91.78% relative to MC and $LR_1$, while the RR system demonstrated reductions of 24.06–47.24%. Additionally, average daily cumulative $CO_2$ emissions from RSR were reduced by 17.01%, and the RR system showed an average reduction of 6.76%, thereby lowering both GWP and GHGI. These results clearly indicate that, irrespective of seasonal or growth duration differences, the RR system maintains superior GHG mitigation capacity compared to both DC and $LR_1$ systems. This advantage stems largely from the unique physiological characteristics of RSR. Specifically, hormonal and other regulatory factors activated during mechanical cutting and ratooning enhance the partitioning of photosynthetic products to aboveground tissues compared to $LR_1$. This promotes sprouting and elongation of axillary buds and facilitates tillering regeneration. As a result, allocation of photosynthates — including NSCs and $^{13}C$ assimilates — to belowground parts is diminished, reducing substrate availability for methane synthesis, decreasing heterotrophic microbial abundance, and increasing autotrophic microbial populations. These shifts contribute to lower direct carbon emissions from RSR, higher daily yields, and improved overall carbon budget balance (Chen *et al.* 2024; Lin *et al.* 2024; Zou *et al.* 2024; Li *et al.* 2025). Prior studies support this mechanism: modulating photosynthate allocation can suppress methane emissions. For instance, introducing the *gs3* or barley SUSIBA2 alleles increases carbon allocation to grains or reduces root dry matter, thereby limiting substrates for methanogens (Su *et al.* 2015; Kwon *et al.* 2023). Transcriptomic evidence from Hu *et al.* (2024) further confirms that preferential carbon partitioning from roots to stems effectively inhibits methanogenesis. Furthermore, RSR cultivation requires only post-harvest water and fertilizer inputs, eliminating the need for seed preparation, seedling nursery management, and transplanting — processes associated with indirect carbon and nitrogen emissions. This enhances the carbon budget surplus and improves resource use efficiency by 87.11–128.16% compared to MC and $LR_1$. In contrast, the DC system necessitates re-tilling of early rice stubble, seedling cultivation, and transplanting for late rice establishment, increasing input and labor demands. Consequently, average daily cumulative $CH_4$ emissions from the RR system were 9.65–35.71% lower than those from the DC system, with carbon and nitrogen footprints reduced by 19.13–36.17% and 19.56–21.53%, respectively. Resource use efficiency thus increased by 35.66–57.53%. Overall, the daily economic return per unit area from RSR was estimated to be 99.13–165.73% higher than that from MC and $LR_1$. The RR system exhibited a 26.88–65.42% improvement over MC and $LR_1$ (as single cropping benchmarks), and outperformed the DC system by 59.61–101.86%.

### 4.2. Carbon budget surplus and economic benefits of RR

The results of this study indicate that agriculture can function as both a source of carbon emissions and an important carbon sink system. Within the context of China's "Dual Carbon" strategy, in-depth research on agricultural carbon

trading represents an emerging approach to synergistically advance carbon sequestration and emission reduction in agriculture while enhancing farmers' incomes. Agricultural carbon trading primarily operates through the Chinese Certified Emission Reduction (CCER) market, which enables farmers to obtain direct economic benefits by participating in carbon mitigation practices during crop production, thereby improving their income levels. The findings demonstrate that the mechanized low-stubble ratoon rice (MC+RSR) system is an environmentally sustainable agricultural model characterized by high yield, efficient carbon sequestration, and reduced emissions. Specifically, the annual carbon budget balance of the RSR exhibited an average increase of 17.49 and 9.09% compared to the MC and $LR_1$, respectively. The RR system showed an average improvement of 117.49 and 102.75% relative to the early-season MC and traditional $LR_1$. The estimated annual average carbon budget surplus for the RR system is 22.38 t $CO_2$-eq $ha^{-1}$, whereas the $LR_1$ system achieves a surplus of 11.23 t $CO_2$-eq $ha^{-1}$, and the DC system reaches 23.77 t $CO_2$-eq $ha^{-1}$. Notably, all three systems function as net carbon sinks. According to data from the National Carbon Market website (https://www.cets.org.cn/), the carbon trading price on March 29, 2025, was 86.13 CNY $t^{-1}$ of $CO_2$. Based on this value, RR, $LR_1$ and DC cultivation is projected to increase farmers' income by 1,697.14–2,357.82 CNY, 768.08–1,160.16 CNY, and 1,998.20–2,096.79 CNY $ha^{-1}$ through carbon trading, respectively (Zhang *et al.* 2023). Thus, the conventional perception that rice systems act as carbon sources contrasts with our findings, likely due to differences in methodological approaches and system boundary definitions. Moreover, most existing studies emphasize carbon emissions while neglecting the carbon fixation potential of various rice cultivars under mechanized farming conditions. In contrast, this study provides a comprehensive assessment by accounting for both direct and indirect GHG emissions — including carbon and nitrogen footprints — across the full life cycle. Additionally, it evaluates the photosynthetic productivity of above-ground rice biomass, incorporating the recycling of rice straw into the field and its contribution to grain yield for human consumption. However, changes in soil carbon storage over the life cycle were not included in this analysis, as annual variations are considered negligible (Lal 2004; Huang *et al.* 2021). Consequently, we conclude that RR constitutes a simplified, low-carbon, and high-efficiency production system. Given the rapid expansion of mechanized RR cultivation, it is recommended that national and regional authorities promptly incorporate the greenhouse gas emission reductions associated with such agricultural practices into official inventory compilation and statistical accounting frameworks. This integration would support and incentivize farmer participation in research and practice adoption, thereby ensuring food security while effectively increasing rural incomes — achieving a high degree of alignment among agricultural ecological, economic, and social benefits.

## 5. Conclusion

This study employed physiological and ecological methods to evaluate the time-based productivity and daily average carbon emissions of RR systems. The results demonstrated that the RR, $LR_1$, and DC systems all functioned as carbon sinks, with respective carbon budget surpluses of 22,380.01, 11,228.54, and 23,772.15 kg $CO_2$-eq $ha^{-1}$, respectively. These findings indicate that RR exhibits a greater carbon sequestration capacity and higher carbon surplus, attributable to its substantially increased average daily yield, lower average daily carbon emissions, and reduced average daily carbon and nitrogen footprints compared to both $LR_1$ and DC systems. Specifically, the average daily yield of RR was 8.03% higher than that of $LR_1$ and 20.81% higher than that of DC. Average daily direct $CO_2$ emissions and indirect $CO_2$ emissions from RR were 15.57 and 12.26% lower, respectively, than those from $LR_1$, and 6.46 and 17.97% lower, respectively, than those from the DC system. Furthermore, the average daily carbon footprint and nitrogen footprint of RR were 24.30 and 4.28% lower, respectively, relative to $LR_1$, and 20.38 and 11.45% lower, respectively, compared to DC. Moreover, the resource utilization efficiency and average daily economic benefits of RR were 24.42 and 32.71% higher, respectively, than those of $LR_1$, and 47.50 and 80.75% higher, respectively, than those of DC. Collectively, these results provide theoretical and practical insights for advancing agricultural carbon neutralization technologies and ensuring food security.

## Acknowledgements

This research was funded by the National Key Research and Development Program of China (2016yfd30300508, 2017YFD0301602, and 2018yfd0301105) and the Science & Technology Development Fund of Fujian Agriculture and Forestry University, China (kf2015043).

## Declaration of competing interest

The authors declare that they have no conflict of interest.

## Declaration of generative AI and AI-assisted technologies in the writing process

The authors declare that they did not use AI in the preparation and writing of this manuscript.

**Appendices** associated with this paper are available at https://doi.org/10.1016/j.jia.2025.07.012

## References

Chen H, Yao F, Yang Y, Zhang Z, Fang C, Chen T, Lin W. 2023. Progress and challenges of rice ratooning technology in Fujian Province, China. *Crop and Environment*, **2**, 121–125.

Chen S, Liu T, Cao C, Ling L, Wang B. 2021. Situation of carbon neutrality in rice production and techniques for low-carbon rice farming. *Journal of Huazhong Agricultural University*, **40**, 3–12. (in Chinese)

Chen S, Zhao Q, Chen H, Jin H. 2019. Genome-wide identification and expression analysis of sucrose synthase family in maize. *Southwest China Journal of Agricultural Sciences*, **32**, 2479–2485. (in Chinese)

Chen T, Weng P, Lan C, Nyumah F, Guo C, Zhang Z, Lin W F, Chen H, Lin W. 2024. Studies and prospectives of mechanically harvested ratooning rice in China. *Technology in Agronomy*, **4**, e015.

Ceschia E, Béziat P, Dejoux J F, Aubinet M, Bernhofer C, Bodson B, Buchmann N, Carrara A, Cellier P, Tommasi P D, Elbers J

A, Eugster W, Grünwald T, Jacobs C M J, Jans W W P, Jones M, Kutsch W, Lanigan G, Magliulo E, Marloie O, *et al.* 2010. Management effects on net ecosystem carbon and GHG budgets at European crop sites. *Agriculture*, *Ecosystems & Environment*, **139**, 363–383.

Deng S. 2024. Investigation and analysis on the current status of ratoon rice production. MSc thesis, Huazhong Agricultural University, China. (in Chinese)

Cui Z, Zhang H, Chen X, Zhang C, Ma W, Huang C, Zhang W, Mi G, Miao Y, Li X, Gao Q, Yang J, Wang Z, Ye Y, Guo S, Lu J, Huang J, Lv S, Sun Y, Liu Y, *et al.* 2018. Pursuing sustainable productivity with millions of smallholder farmers. *Nature*, **555**, 363–366.

Fang F, Cheng S. 2018. Rice technology and industrial development. *Acta Agronomica Sinica*, **8**, 92–98. (in Chinese)

Hu J, Bettembourg M, Xue L, Hu R, Schnürer A, Sun C, Jin Y, Sundström J F. 2024. A low-methane rice with high-yield potential realized via optimized carbon partitioning. *Science of the Total Environment*, **920**, 170980.

Huang J, Pan Y, Chen H, Zhang Z, Fang C, Shao C, Amjad H, Lin W. 2020. Physiochemical mechanisms involved in the improvement of grain-filling, rice quality mediated by related enzyme activities in the ratoon cultivation system. *Field Crops Research*, **258**, 107962.

Huang J, Yu X, Zhang Z, Peng S, Liu B, Tao X, He A, Deng N, Zhou Y, Cui K, Wang F, Huang J L. 2022. Exploration of feasible rice-based crop rotation systems to coordinate productivity, resource use efficiency and carbon footprint in Central China. *European Journal of Agronomy*, **141**, 126633.

Huang W, Wu J, Pan X, Tan X, Zeng Y, Shi Q, Liu T, Zeng Y. 2021. Effects of long-term straw return on soil organic carbon fractions and enzyme activities in a double-cropped rice paddy in South China. *Journal of Integrative Agriculture*, **20**, 236–247.

IPCC (Intergovernmental Panel on Climate Change). 2013. Climate Change 2013: The Physical Science Basis. In: Stocker T F, Qin D, Plattner G K, Tignor M, Allen S K, Boschung J, Nauels A, Xia Y, Bex V, Midgley P M, eds., *Contribution of Working Group I to the Fifth Assessment Report of the Intergovernmental Panel on Climate Change*. Cambridge University Press, UK.

Jiang Y, Guan D, Zhang W. 2018. The effect of rice plant traits on methane emissions from paddy fields: A review. *Chinese Journal of Eco-Agriculture*, **26**, 175–181. (in Chinese)

Jiang Y, Zhu X, Qian H, Zhang N, Ding Y. 2022. Higher rice yields and lower methane emissions can be reconciled for rice cultivation: A review. *Journal of Nanjing Agricultural University*, **45**, 839–847. (in Chinese)

Kwon Y, Lee J Y, Choi J, Lee S M, Kim D, Cha J K, Park H, Kang J W, Kim T H, Chae H G, Kabange N R, Oh K W, Kim P J, Kwak Y S, Lee J H, Ryu C M. 2023. Loss-of-function *gs3* allele decreases methane emissions and increases grain yield in rice. *Nature Climate Change*, **13**, 1329–1333.

Lal R. 2004. Soil carbon sequestration impacts on global climate change and food security. *Science*, **304**, 1623–1627.

Li J, Qin B, Lan C, Xu H, Zou J, Zhang B, Fang C, Zhang Z, Chen H, Lin W. 2025. Rhizosphere microecological mechanism of carbon sequestration and its emission mitigation in rice ratooning. *Agriculture*, *Ecosystems & Environment*, **381**, 109406.

Li P, Liu J, Saleem M, Li G, Luan L, Wu M, Li Z. 2022. Reduced chemodiversity suppresses rhizosphere microbiome functioning in the mono-cropped agroecosystems. *Microbiome*, **10**, 1–15.

Li R, Tian Y, Wang F, Sun Y, Lin B, Dang Y P, Zhao X, Zhang H, Xu Z. 2024. Optimizing the rate of straw returning to balance trade-offs between carbon emission budget and rice yield in China. *Sustainable Production and Consumption*, **47**, 166–177.

Li Y, Zheng W, Xiao X, Huang T, Xiao F, Lu W, Han D, Liu X, Chen M, Dai X, Wang R, Liu K, Xiao G. 2021. Effects of mechanical harvesting stubble heights on grain yield of ratoon rice under the triple-cropping system of rape–rice–ratoon rice in the area of red soil paddy of northcentral Jiangxi. *Hybrid Rice*, **36**, 87–92. (in Chinese)

Lin F, Rensing C, Pang Z, Zou J, Lin S, Letuma P, Zhang Z, Lin W. 2022. Metabolomic analysis reveals differential metabolites and pathways involved in grain chalkiness improvement under rice ratooning. *Field Crops Research*, **283**, 108521.

Lin Q, Cai Q, Cui L, Jiang Z, Jiang J, Wu F, Luo X, Xiao Y, Xie H, Zhang J. 2022. Research progress on screening and breeding of ratoon rice varieties. *China Rice*, **28**, 1–6. (in Chinese)

Lin Q, Zheng C, Lin Q, Zhu Y, Wang Y, Jiang J, Jiang Z, Zhang J, 2021. Relationships of panicle to stem ratio with yield and its components of ratoon rice. *Journal of Northwest A&F University* (Nat. Sci. Ed.), **49**, 65–74. (in Chinese)

Lin W X. 2019. Developmental status and problems of rice ratooning. *Journal of Integrative Agriculture*, **18**, 246–247.

Lin W, Chen H, Zhang Z, Xu Q, Mei T N, Fang C, Ren W. 2015. Research and prospect of physiological and ecological characteristics of ratoon rice yield formation and key cultivation techniques. *Chinese Journal of Eco-Agriculture*, **23**, 392–401. (in Chinese)

Lin W, Weng P, Lin W F, Shao C, Guo C, Chen H, Chen T. 2024. Research status and prospect of ratoon rice in China under mechanically harvested condition. *Chinese Journal of Applied Ecology*, **35**, 827–836. (in Chinese)

Lin Z, Li Z, Wen P, Wu D, Zou J, Pang Z, Lin W. 2022. Field greenhouse gas emission characteristics and carbon footprint of ratoon rice. *Chinese Journal of Applied Ecology*, **33**, 1340–1351. (in Chinese)

Ling X, Zhang T, Deng N, Yuan S, Yuan G, He W, Cui K, Nie L, Peng S, Li T, Huang J. 2019. Modelling rice growth and grain yield in rice ratooning production system. *Field Crops Research*, **241**, 107574.

Liu J. 2019. Effects of high temperature on grain starch size distribution, sucrose degradation, and storage protein accumulation metabolism in rice (*Oryza sativa* L.). MSc thesis, Zhejiang University, Cnina. (in Chinese)

Tang J, Liu T, Yang J, Nie J, Xing J, Zhang L, Zhang W, Tan W, Cao C. 2022. Current status of carbon neutrality in Chinese rice fields (2002–2017) and strategies for its achievement. *The Science of the Total Environment*, **842**, 156713.

Mandal U K, Bhardwaj A K, Lama T D, Nayak D B, Burman D, Samui A, Mahanta K K, Sarangi S K, Mandal S, Raut S. 2021. Net ecosystem exchange of carbon, greenhouse gases, and energy budget in coastal lowland double cropped rice ecology. *Soil and Tillage Research*, **212**, 105076.

Nakano H, Tanaka R, Nakagomi K, Hakata M. 2021. Grain yield response to stubble leaf blade clipping in rice ratooning in southwestern Japan. *Agronomy Journal*, **113**, 4013–4021.

Qian H, Yuan Z, Chen N, Zhu X, Huang S, Lu C, Liu K, Zhou F, Smith P, Tian H, Xu Q, Zou J, Liu S, Song Z, Zhang W, Wang S, Liu Z, Li G, Shang Z, Ding Y, *et al.* 2025. Legacy effects cause systematic underestimation of $N_2O$ emission factors. *Nature Communications*, **16**, 2775.

Qian H, Zhu X, Huang S, Linquist B, Kuzyakov Y, Wassmann R, Minamikawa K, Martinez-Eixarch M, Yan X, Zhou F, Sander B O, Zhang W, Shang Z, Zou J, Zheng X, Li G, Liu Z, Wang S, Ding Y, van Groenigen K J, *et al.* 2023. Greenhouse gas emissions and mitigation in rice agriculture. *Nature Reviews Earth & Environment*, **4**, 716–732.

Qu X, Ren Y, Wang H, Zhang J, Xie Y. 2020. Report on the changes in the main characteristics of cultivated land quality in China over the past 30 years. *China Comprehensive Agricultural Development*, **5**, 25–26. (in Chinese)

Ren X, Cui K, Deng Z, Han K, Peng Y, Zhou J, Zhai Z, Huang J, Peng S. 2023. Ratoon rice cropping mitigates the greenhouse effect by reducing $CH_4$ emissions through reduction of biomass during the ratoon season. *Plants*, **12**, 3354.

Shi W, Zhu G, Sun M, Wang A, Chen Z, Yan G. 2020. Influence factors and mechanism of rice grain filling: Research progress. *Chinese Agricultural Science Bulletin*, **36**, 1–7. (in Chinese)

Smith P, Lanigan G, Kutsch W L, Buchmann N, Eugster W, Aubinet M, Ceschia E, Béziat P, Yeluripati J B, Osborne B, Moors E J, Brut A, Wattenbach M, Saunders M, Jones M. 2010. Measurements necessary for assessing the net ecosystem carbon budget of croplands. *Agriculture*, *Ecosystems & Environment*, **139**, 302–315.

Song K, Zhang G, Yu H, Xu H, Lv S, Ma J. 2021. Methane and nitrous oxide emissions from a ratoon paddy field in Sichuan Province, China. *European Journal of Soil Science*, **72**, 1478–1491.

Su J, Hu C, Yan X, Jin Y, Chen Z, Guan Q, Wang Y, Zhong D, Jansson C, Wang F, Schnürer A, Sun C. 2015. Expression of barley SUSIBA2 transcription factor yields high-starch low-methane rice. *Nature*, **523**, 602–606.

Wei J, Xu H, Zhou L, Cheng X, Tang X, Fu Z, Tang Q, Tang J. 2018. Seasonal variation in carbon exchange and its modulating factors

of a double cropping rice ecosystem in Southern China. *Journal of Agro-Environment Science*, **37**, 1035–1044. (in Chinese)
Wang F, Peng S. 2018. Research progress in rice green and high-yield management practices. *Chinese Bulletin of Life Sciences*, **30**, 1129–1136. (in Chinese)
Wang W, He A, Jiang G, Sun H, Jiang M, Man J, Nie L. 2020. Ratoon rice technology: A green and resource-efficient way for rice production. *Advances in Agronomy*, **159**, 135–167.
Wang Y. 2021. Effects of nitrogen management on yield formation of ratoon rice and the related mechanism. Ph D thesie, Huazhong Agricultural University, China. (in Chinese)
Xu C, Ji L, Chen Z, Fang F. 2018. Trends of green development of rice production in China. *Chinese Bulletin of Life Sciences*, **30**, 1146–1154. (in Chinese)
Xu F, Xiong H, Zhang L, Zhu Y, Jiang P, Guo X, Liu M. 2015. Progress in research of yield formation of ratooning rice and its high-yielding key regulation technologies. *Scientia Agricultura Sinica*, **48**, 1702–1717. (in Chinese)
Xu Y, Liang L, Wang B, Xiang J, Gao M, Fu Z, Long P, Luo H, Huang C. 2022. Conversion from double-season rice to ratoon rice paddy fields reduces carbon footprint and enhances net ecosystem economic benefit. *Science of the Total Environment*, **813**, 152550.
Yang D, Peng S, Qi M, Xiong Z, Deng S, Wang F. 2023. Comparison of grain cadmium and arsenic concentration between main and ratoon crop in rice ratooning system. *Food Chemistry*, **399**, 134017.
Yao L, Lai Y, Zhao M. 2024. Paths to enhance farmers' income by agricultural carbon trading. *Journal of Huazhong Agricultural University*, **43**, 9–16. (in Chinese)
Yoshida S, Forno D A, Cock J H. 1971. *Laboratory Manual for Physiological Studies of Rice*. International Rice Research Institute, Los Baños, Laguna.
Yu J, Kees Jan V G, Shan H, Bruce A H, Chris V K, Hu S, Zhang J, Wu L, Yan X, Wang L, Chen J, Hang X, Zhang Y, Horwath W R, Ye R, Linquist B A, Song Z, Zheng C, Deng A, Zhang W. 2017. Higher yields and lower methane emissions with new rice cultivars. *Global Change Biology*, **23**, 4728–4738.
Yu X, Xu L, Yuan S, Yang G, Xiang H, Fu Y, Huang J, Peng S. 2023. Resource use efficiencies, environmental footprints and net ecosystem economic benefit of direct-seeded double-season rice in Central China. *Journal of Cleaner Production*, **393**, 136249.
Yu X, Yuan S, Tao X, Huang J, Yang G, Deng Z, Xu L, Zheng C, Peng S. 2021. Comparisons between main and ratoon crops in resource use efficiencies, environmental impacts, and economic profits of rice ratooning system in Central China. *Science of the Total Environment*, **799**, 149246.
Yuan S, Cassman K G, Huang J, Peng S, Patricio G. 2019. Can ratoon cropping improve resource use efficiencies and profitability of rice in Central China? *Field Crops Research*, **234**, 66–72.
Yuan S, Yang C, Yu X, Zheng C, Xiao S, Xu L, Cui K, Huang J, Peng S. 2022. On-farm comparison in grain quality between main and ratoon crops of ratoon rice in Hubei Province, Central China. *Journal of the Science of Food and Agriculture*, **102**, 7259–7267.
Zhang H, Hu Y, Yang J, Dai Q, Huo Z, Xu K, Wei H, Gao H, Guo B, Xing Z, Hu Q. 2021. Development and prospect of rice cultivation with Chinese characteristics. *Chinese Agricultural Science*, **54**, 1301–1321. (in Chinese)
Zhang W, Shang Z, Zhang J, Yan S, Deng A, Zhang X, Zheng C, Song Z. 2023. Standardized establishment and improvement of accounting system of agriculture greenhouse gas emission. *Scientia Agricultura Sinica*, **56**, 4467–4477. (in Chinese)
Zhao F, Yang P, Gao Q, Xia L, Fan L, Hu M. 2024. Effects of the long-term rice expansion on ecosystem carbon budget in the typical agricultural area of Northeast China. *Sustainable Production and Consumption*, **52**, 613–623.
Zou J N, Pang Z Q, Li Z, Guo C L, Lin H M, Li Z, Chen H F, Huang J W, Chen T, Xu H L, Qin B, Letuma P, Lin W W, Lin W X. 2024. The underlying mechanism of variety–water–nitrogen–stubble damage interactions on yield formation in ratoon rice with low stubble height under mechanized harvesting. *Journal of Integrative Agriculture*, **23**, 806–823.

Executive Editor-in-Chief Shaokun Li
Managing Editor Ning Wang